NASA TM X-1721

ROCKET ENGINE EVALUATION OF EROSION AND CHAR AS FUNCTIONS OF FABRIC ORIENTATION FOR SILICA-REINFORCED NOZZLE MATERIALS

by Donald A. Peterson, Jerry M. Winter,
and Arthur M. Shinn, Jr.

Lewis Research Center
Cleveland, Ohio

DISCLAIMER NOTICE

THIS DOCUMENT IS BEST
QUALITY AVAILABLE. THE
COPY FURNISHED TO DTIC
CONTAINED A SIGNIFICANT
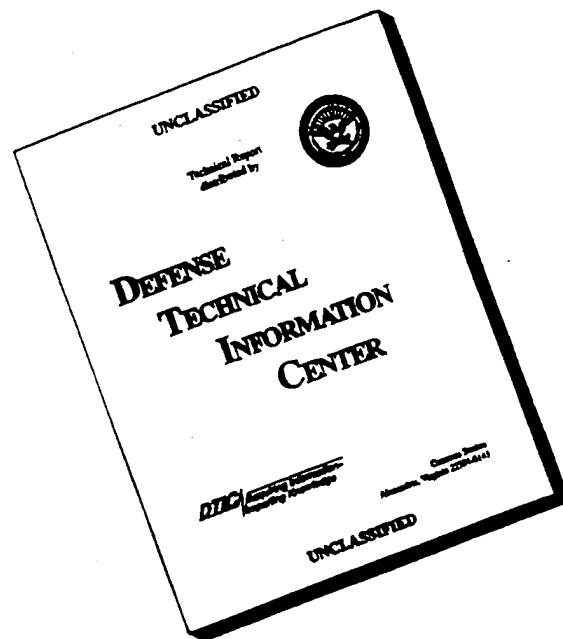NUMBER OF PAGES WHICH DO
NOT REPRODUCE LEGIBLY.

ROCKET ENGINE EVALUATION OF EROSION AND CHAR AS FUNCTIONS

OF FABRIC ORIENTATION FOR SILICA-REINFORCED

NOZZLE MATERIALS

By Donald A. Peterson, Jerry M. Winter, and Arthur M. Shinn, Jr.

Lewis Research Center
Cleveland, Ohio

ABSTRACT

Thirty-five silica reinforced ablative specimens were evaluated. Quartz reinforcement was determined to have the greatest resistance to erosion, but a low-cost silica powder-filled material was also high in erosion resistance. A fabric orientation of 60° to the nozzle centerline resulted in low char depth and high erosion resistance. The fabric layup angle to the gas stream should be minimized to minimize char depth and reduce engine weight. A 0° helix angle used for rosette layups resulted in delaminations and severe erosion.

ROCKET ENGINE EVALUATION OF EROSION AND CHAR AS FUNCTIONS OF

FABRIC ORIENTATION FOR SILICA-REINFORCED NOZZLE MATERIALS

by Donald A. Peterson, Jerry M. Winter, and Arthur M. Shinn, Jr.

Lewis Research Center

SUMMARY

Thirty-five silica reinforced ablative specimens were evaluated as nozzle sections of a storable propellant (nitrogen tetroxide and a blend of 50-percent unsymmetrical dimethyl-hydrazine and 50-percent hydrazine) rocket engine. Testing was performed at an oxidant-to-fuel ratio of 1.6, a chamber pressure of 100 psia (689 kN/m^2), an initial throat diameter of 7.82 inches (19.8 cm), and a run duration of 150 seconds. Both oxidant-to-fuel ratio and chamber pressure were maintained constant during the test firing. Ten materials and five fabric orientations were evaluated.

Quartz reinforcement was determined to have the greatest resistance to erosion, but a low-cost silica powder-filled material was also high in erosion resistance. For most of the materials tested, a fabric orientation of 60° to the nozzle centerline resulted in low char depths and high resistance to erosion. A 0° helix angle used for the rosette layup resulted in delaminations and severe erosion. The fabric layup angle to the gas stream should be minimized to minimize char depth and reduce engine weight. A 0° angle cannot be used because of delaminations; however, a rosette layup gives the effect of minimum angle to the gas stream.

INTRODUCTION

Ablative materials are used extensively to provide sacrificial cooling in a number of liquid and solid propellant rocket engine applications. Advantages of ablative cooling include simplicity, reliability, ease of fabrication, and compatibility with deep throttling requirements. Literally hundreds of composite ablative materials are available to the design engineer. For any particular application, he must finally choose the one material

system he thinks is most suitable for the intended mission. His first consideration must be reliability. After satisfying structural integrity requirements, he can explore methods of increasing performance and minimizing engine weight.

The use of a particular class of ablative reinforcement material will generally be dictated by the propellant combination, and a thermal stress analysis can help to determine the desired physical properties. The use of various resins and filler systems is generally determined by the thermal load imposed by the duty cycle and chamber geometry. Proper variation in resin compounding and fabrication techniques can also improve ablative characteristics.

Computer programs and plasma jet simulators are sometimes used to predict or confirm reliability and performance of materials in a particular combustion environment. Unfortunately, such techniques have not been completely successful. They suffer from an inability to discriminate quantitatively the very many interrelations between a material and its environment. The inputs to computer programs are also handicapped by insufficient physical property data. Qualitative relations or gross effects can be predicted, and are useful for initial screening purposes. Prior to a final material selection, however, subscale testing is usually employed. In this manner, a close approximation to the actual combustion environment and duty cycle can be attained.

Some of the major material and processing variables affecting the erosion resistance of silica reinforced materials as nozzle sections of a 7.8-inch (19.8-cm) throat diameter storable propellant rocket engine are reported in reference 1. The results of that investigation suggested that it is possible to optimize an ablative composite to meet the requirements of a range of storable propellant rocket engine duty cycles. The present investigation is concerned with defining the interrelations of erosion resistance and char growth as functions of the fabric layup angle. The application of this information should help the designer to minimize engine weight while maintaining high performance.

The sum of material erosion and char can be used as a measure of overall effectiveness. In this manner, all insulation necessary to perform a particular duty cycle is included as total required weight. Of course, neither of these variables must be allowed to exceed a critical value which would jeopardize mission requirements.

A total of 35 nozzles was tested. Ten materials and five fabric orientations were studied. The nominal engine conditions included an oxidant-to-fuel ratio of 1.6, constant chamber pressure of 100 psia (689 kN/m^2), and an initial throat diameter of 7.82 inches (19.8 cm). Each test firing was conducted at an ambient pressure of 1.6 psia for a run duration of 150 seconds. The results are presented in terms of throat radius change and amount of char experienced for each nozzle. Comparisons are made for identical materials at different fabric layup angles, and also for different materials at constant layup angles.

2

APPARATUS

ABLATIVE MATERIAL SAMPLES

Ten different materials were tested (table I). Eight contained high silica fabric as the reinforcement and two used quartz fabric as the reinforcement material. Five fabric orientations are included, A through E. A defines a fabric layup at 30° to the nozzle centerline; B, 60°; and C, 90°. (The angle to the nozzle centerline is measured upstream.) The D designation refers to material molded from 1/2- by 1/2-inch (1.27- by 1.27-cm) squares randomly oriented. The rosette type layup, described in reference 1, is identified by the letter E.

The rosette nozzles were laid up in a female tool using a 0° helix angle and hydroclaved at 1000 psia (6894 kN/m^2) pressure. The remaining nozzles were compression molded at 1000 psia (6894 kN/m^2).

FACILITY

The experimental test runs were conducted in the Propulsion Systems Laboratory altitude facility shown in figure 1. A view of the test chamber area is shown in figure 2. A test engine mounted to the thrust stand and the entrance to the exhaust collector can be seen.

The fuel (50-50 blend of UDMH and hydrazine) run tank had a capacity of 560 gallons (2.54 m^3) while the oxidant (N$_2$O$_4$) run tank capacity was 707 gallons (3.21 m^3). A capability for over 400 seconds continuous operation was, therefore, possible at a chamber pressure of 100 psia (689 kN/m^2), an oxidant-to-fuel ratio of 1.6, and a constant throat diameter of 7.82 inches (19.8 cm).

Engine combustion products were passed through a water-cooled collector and cooled by heat exchangers before being exhausted to the atmosphere approximately 80 feet (24.4 m) above ground level.

ENGINE

The basic engine, common to all tests, consisted of an injector as shown in the photograph of figure 3, a water-cooled combustion chamber detailed in figure 4, and the test nozzle shown in figure 5.

The injector used throughout the entire testing program was fabricated with 127 triplet elements arranged in a circular pattern. Each element had two fuel streams, 0.043-inch (0.109-cm) diameter, impinging on one oxidant stream of 0.0785-inch (0.199-cm) di-

ameter. The impingement distance was 0.56 inch (1.42 cm) at an included angle of 20° between the fuel and oxidizer. The nominal oxidant and fuel injection differential pressures were 40 and 50 psia, respectively.

The water-cooled combustion chamber was 20.0 inches (50.8 cm) long and had an inside diameter of 10.78 inches (27.40 cm). The chamber was made of copper with a 0.005-inch (0.0127-cm) coating of nickel to increase resistance to the corrosive environment. A water inlet pressure of 200 psia (1378 kN/m^2) provided a coolant flow rate of 350 gallons per minute (0.0265 m^3/sec).

The ablative test nozzle was bonded into a steel housing and the assembly then bolted to the water-cooled chamber. An epoxy sealant was used, both as the bonding agent and also to provide a hot gas seal at the chamber-nozzle interface.

The basic engine assembly was 23.0 inches (58.5 cm) long, from injector to nozzle throat, and had an L* of 43.0 inches (113 cm) with a contraction ratio of 1.90 and an expansion ratio of 1.30. The nozzle entrance half angle was 30° converging to a 7.82-inch (19.8-cm) throat and expanding at a half angle of 15°.

INSTRUMENTATION

The combustion chamber pressure was obtained using two holes drilled into the injector face and connected to strain gage type pressure transducers. Flow rates for each propellant were measured by two turbine-type flowmeters in series. Thrust was measured by a double bridge strain gage load cell. Thermocouples were installed in both propellant lines and injector domes. A water-cooled flush-mounted pressure transducer was installed on the inside diameter of the combustion chamber to monitor combustion instability.

RECORDING AND PROCESSING

Electrical outputs were sampled at a rate of 4000 samples per second, digitized, and recorded on magnetic tape by the central data system. Selected outputs were also recorded by multichannel oscillograph and strip chart recording instruments for control room data reduction and system monitoring. The data on magnetic tape was first checked on an oscilloscope display unit and then introduced into a computer along with the appropriate calibration and conversion constants for processing. The output data were printed at one-second intervals.

4

PROCEDURE

TESTING

The operation of the instrumentation was verified and the engine assembly pressure checked prior to each run. The propellant run tanks were loaded and pressurized with nitrogen gas. The closed loop controller was set to maintain a constant chamber pressure of 100 psia (689 kN/m^2) and an oxidant-to-fuel ratio of 1.6 during each firing. Changes in chamber pressure, due to throat area change, were continuously compensated by corresponding changes in the propellant flow rate. The altitude chamber was evacuated to approximately 1.60 psia (11 kN/m^2) pressure and the high-pressure pumps were activated to supply cooling water to the chamber. A sequence timer automatically activated appropriate valves, data acquisition equipment, and propellant line purges for each run. An oscilloscope was used to monitor possible combustion instability. A manual abort switch would be used to end the test 1 or 2 seconds after detection of any high frequency instability.

All ablative nozzles were subjected to a continuous firing duration of 150 seconds. The throat diameter of all nozzles was measured before and after testing with a micrometer. After cooldown, each nozzle was sectioned. Measurements of char thickness and virgin ablative material remaining after the firing were obtained for percent char-through calculation. The entrance, throat, and exit planes were measured. All nozzles had identical orientation with respect to the injector during the run and were sectioned in the same location after the firing to minimize bias from nonuniform gas temperature distribution. Therefore, all measurements were made from nozzles fired for 150 seconds under essentially identical conditions. The reported value of the char (original virgin minus remaining virgin) includes a portion of material lost due to erosion and is, therefore, a measure of the overall thickness required for the various ablative materials and fabric orientations to complete a 150-second continuous firing. A full-length photograph of each sectioned nozzle was also taken.

The combustion performance was evaluated periodically during the course of the program to check for possible injector deterioration by substituting a heat-sink nozzle for the ablative nozzle sections and conducting short duration firings over an oxidant-to-fuel range of 1.4 to 2.0. The heat-sink nozzle geometry was similar to that of the ablative nozzle (fig. 5) except the entrance section used a radius of curvature (7.82 in. (19.8 cm)) instead of the 30° angle of the ablative.

CALCULATIONS

The combustion performance level as expressed by the characteristic velocity efficiency was based on vacuum specific impulse obtained from thrust and propellant flow measurements. The equations used were as follows:

$$\text{Vacuum thrust} = F_v = F_m + P_o A_{ex}$$

where F_m is the measured thrust, P_o is the ambient pressure, and A_{ex} is the area at the nozzle exit plane.

$$I_v = \frac{F_v}{\dot{W}}$$

where I_v is the experimental vacuum impulse and $\dot{W}$ is the total propellant weight flow.

$$\eta_{I_v} = \frac{I_v}{I_{v,th}}$$

where η_{I_v} is the vacuum impulse efficiency, and subscript th is the theoretical shifting equilibrium vacuum impulse.

$$\eta_{C^*} = \frac{\eta_{I_v}}{\eta_{C_{F_v}}} = \frac{\eta_{I_v}}{0.983}$$

where η_{C^*} is characteristic velocity efficiency and 0.983 is the calculated nozzle thrust-coefficient efficiency.

Characteristic velocity efficiency calculations were also made, based on injector end chamber pressure and propellant flow measurements.

$$C^* = \frac{(0.946)(P_c)(g)(A_T)(C_D)}{\dot{W}}$$

In this equation C^* is characteristic velocity, P_c is the measured injector end pressure, $\dot{W}$ is the total propellant flow rate, g is the gravitational constant, A_T is the nozzle throat area, and C_D is the nozzle discharge coefficient (0.994). The factor 0.946 (ref. 2) accounts for the momentum pressure loss when applied to the injector end meas-

6

urement. This correction factor of 0.946 was obtained from reference 2 by a total pressure probe inserted into the exit end of the heat-sink nozzle and located on the nozzle centerline at the throat plane.

Two methods were used to determine the radius change of the ablative nozzle as a function of run time: (1) average throat diameter measurements by micrometer before and after each run, and (2) the throat radius as defined by A_t in the equation for C^*. The experimental characteristic exhaust velocity, calculated from thrust on the heat-sink engines, is used together with the corrected injector end chamber pressures and the total propellant flow. Solving for throat radius change ΔR_T at any time during the run gives

$$\Delta R_T = \left[\sqrt{\frac{C^* \dot{W}}{\pi(g)(C_D)(P_c)(0.946)}} - R_{T_o} \right] \times 10^3$$

which is the radius change in mils. The symbol R_{T_o} refers to the initial throat radius at time zero. The precision of the radius change calculation was estimated to be ±0.008 inch (±0.0203 cm) at a 95 percent confidence level. The propellant flow method was programmed into the computer to facilitate data reduction, to standardize the method of ablative material evaluation, and to obtain radius change as a function of run time.

The equation used to calculate percent char-through was

$$\text{Percent char-through} = \frac{ABLi - ABL_f}{ABLi} \times 100$$

where $ABLi$ is the initial ablative thickness and ABL_f is the final thickness of the uncharred ablative material after the firing. The thickness of the asbestos insulation (see fig. 5) was not used in the calculation so as to reflect the insulative properties of the ablative material only.

RESULTS AND DISCUSSION

CHARACTERISTIC VELOCITY EFFICIENCY

The variation of erosion rate with small changes in injector performance is very significant and, therefore, it was essential to maintain constant characteristic velocity efficiency throughout the program. Of equal importance was the need to obtain a relatively high value of combustion efficiency as it is possible to experience no dimensional ablation

if the injector efficiency is too low. A C* efficiency of 0.972±0.002 was obtained from thrust and also from the corrected chamber pressure during the heat-sink runs. The value calculated for all ablative runs, obtained from thrust after the initial 5 seconds of each test, was 0.972±0.004. The characteristic velocity efficiency calculated from thrust measurements was maintained at 0.972 throughout the entire test program, indicating no deterioration of the injector.

ABLATIVE MATERIAL NOZZLE FIRINGS

The firing results for all the ablative material nozzles are discussed in three sections. The first section compares the erosion of each material as a function of the reinforcement layup angle. The second section compares the erosion resistance of all materials at a specific layup angle. In the third section, the charring characteristics or insulating efficiency are evaluated in terms of layup angle versus percent char. In addition to the char evaluated at the throat location, the percent char was also plotted for the entrance and exit planes of the nozzle.

Erosion, delamination, and char are shown for each nozzle section in the photographs of figure 6. Table I is a summary of all the materials tested. Although the nozzle entrance half angle was 30°, a fabric orientation of 30° was evaluated to assess the delamination characteristics of a layup angle of 0° to the gas flow. Listed are the material, erosion, and char data for each nozzle tested. Table II lists the nozzles in decreasing order of erosion resistance, and also gives the percent char through at the throat plane.

Effect of Fabric Orientation on Erosion

Seven commonly used silica-phenolic materials were chosen to study fabric orientation. Each of the commonly used materials was evaluated in four or five fabric orientations. The eighth material, compounded with an experimental resin system, was evaluated in two fabric orientations. The ninth material, with quartz reinforcement, was evaluated in 90° orientation; and the tenth material, with quartz reinforcement, was evaluated in the rosette orientation.

A typical erosion curve is shown on figure 7 along with the data spread for all the nozzles tested except those which delaminated. The shape of the curve indicates steady-state erosion has been attained. A significant increase in slope would be expected when the material is completely charred. Therefore, care must be exercised in extrapolating these data.

The bar graphs of figures 8 present the erosion data for all the materials. Total

throat radius change after 150 seconds of firing time was used to compare nozzles. The relative ranking of materials for erosion resistance does not change once steady-state charring has been established.

The erosion data for material number 1, 30-percent phenolic high silica, are presented in figure 8(a). Five fabric orientations were evaluated. With the exception of the rosette layup, all of the fabric orientations gave comparable results. (The possible reasons for the relatively poor erosion resistance of all the rosette nozzles will be discussed later in this section.) However, a slight advantage was noted for the 60° and random square orientations.

Figure 8(b) shows the results for material number 2. This material is a 31-percent phenolic high-silica material which contains 8-percent silica powder as a filler. The 30° and 60° orientations were superior in erosion resistance when compared to the 90° and random square orientations. The nozzle with 30° orientation was delaminated upstream of the throat, but did not extend to the throat (see fig. 6(f)). This may have affected the throat erosion, possibly by changing the aerodynamic characteristics of the throat.

The results for material number 3, a 32-percent phenolic-polyamide resin with high-silica reinforcement, presented in figure 8(c), are similar to those of material 2. The 30° and 60° orientations were superior in erosion resistance to the 90° and random square orientation. The nozzle with 30° orientation was also delaminated upstream of the throat (see fig. 6(j)).

Number 4 material, 20-percent phenolic-polyamide high silica, had fairly uniform erosion results for all of the orientations except the rosette layup which eroded 50-percent more than the other orientations for the same firing duration. The 30° and rosette orientations were also severely delaminated. Material 4a delaminated upstream only while 4e delaminated in the throat region. Figure 8(d) shows the firing results and figures 6(n) and 6(r) are the post-firing photographs which show the fabric delaminations.

Material 5 was a 30-percent phenolic with high-silica - 3-percent chrome salt reinforcement. Figure 8(e) presents the firing results for all the orientations. The erosion was about the same for all layup angles with the exception of the rosette which exhibited considerably less erosion resistance.

Figure 8(f) shows the erosion of material 6, a 30-percent modified phenolic with high-silica reinforcement. The 60° fabric orientation had slightly better erosion resistance when compared to all of the other fabric orientations. The 30° layup angle material exhibited severe upstream delamination (fig. 6(x)).

Material 7 was a high silica reinforcement containing 40-percent phenyl-silane resin and elastomer. The 30° and rosette orientations were severely delaminated. The 30° and 60° fabric orientations both were superior in erosion resistance of the four orientations tested (see fig. 8(g)). The rosette layup had more than 100 percent greater erosion than the 30° or 60° orientations. Post-test photographs may be seen in figures 6(bb) to

9

(ee). A possible cause of the high erosion of all rosette layups may be illustrated by comparing the rosette layup used in reference 1 to the rosette layup used here. A helix angle of approximately 20° is illustrated in figure 6(ee), above. Figure 6(ee), below, shows a helix angle near 0° for nozzle 7E. This was typical of all the rosette nozzles. The lack of helix angle also caused the delamination problems experienced with nozzles 4E and 7E.

The material used for nozzle 8B and 8C was a high-silica fabric impregnated with an experimental high-temperature phenolic type resin. The erosion results are shown in figure 8(h). The 60° orientation exhibited 25 percent greater erosion resistance than the 90° orientation. Posttest photographs are shown in figures 6(ff) and (gg).

Quartz fabric was used for nozzles 9C and 10E. Nozzle 9C was impregnated with a polyimide resin while 10E used a standard type phenolic. The erosion data are presented in figure 8(i). Low erosion rates were obtained, as would be expected with the quartz material (ref. 3) and the 90° orientation angle. The considerably higher erosion for the rosette orientation was most likely due to the orientation of the rosette layup rather than the phenolic resin being appreciably inferior to the polyimide resin.

Figure 9 shows the relative trends for each layup angle. The bar graph represents the average of all materials tested. The total erosion of all the nozzles tested is shown, except the quartz-reinforced nozzles. The greatest resistance to throat erosion was measured with the 60° centerline orientation. Results for a 30° centerline orientation were relatively good but may have been influenced by delamination and loss of material upstream of the nozzle throat. A fabric orientation slightly higher than 30° is required when the nozzle approach angle is 30°.

The unexpectedly poor showing (see ref. 1) of the rosette layup was probably due to the lack of a spiral or helix angle at the throat in these nozzles. Without a helix angle, it is difficult to obtain high interlaminar bond strength together with high overall part density. Decreased shear force resistance results in ply separation and fabric chunking (see fig. 6(ee)).

Effect of Material Variation on Erosion

Figure 10(a) presents the erosion data for the 30° orientation of materials 1 through 7. Despite delamination upstream of the throat, which probably helped reduce throat erosion, the MX-2600(2A) material was superior in erosion resistance to all other materials tested at this fabric orientation. Nozzles 1A (MX-89) and 5A (MXS-141) were the only ones that did not delaminate during the firing. All other materials delaminated during the firing as is indicated in figure 10(a). A 30° orientation of the fabric to the nozzle centerline cannot be used when the entrance half angle of the nozzle is 30° or more. This results in a 0° orientation to the hot gas flow and is responsible for fabric delamination.

10

The relatively low erosion rates of the 30° orientation nozzles was most likely due to delaminations upstream of the throat which may have changed the aerodynamic characteristics of the throat and protected the throat plane from erosion.

A meaningful comparison of materials is difficult because of the delaminations. A layup angle slightly greater than 30° might have prevented the delaminations.

The erosion data for the materials laid up 60° to the nozzle centerline is presented in figure 10(b). Nozzles 2B and 3B (MX-2600 and MX-19) had the greatest resistance to erosion. The least erosion resistant material, 5B (MX-141), was similar in construction to 3B, except for a small percentage of chromium salts added to the fabric of 5B. The wide difference in erosion resistance was not expected for these two materials, nor was 3 material expected to be superior to 5 (ref. 1). The 60° orientation provided erosion resistance equal to, or better than, the other fabric orientation for eight of the nine materials evaluated. The only exception was material 4 (MX-87) which was low in resin content (20 percent).

Figure 10(c) compares the erosion resistance of all the materials laid up at 90° to the nozzle centerline. Material 9C, quartz reinforced, was superior in erosion resistance to all other materials tested by a wide margin. For this orientation, the similar materials, 3C (MX-19) and 5C (MXS-141), were approximately equivalent in erosion resistance. The 90° orientation gave the best erosion resistance for material 4 (MX-87). It appears that to provide adequate cooling for low resin content ablatives, the decomposed resin gases must be injected most efficiently into the boundary layer. The 90° orientation apparently allowed better utilization of the coolant gases than the 60° orientation for the low resin content ablative material. The lowest cost material, 2C (MX-2600), was also reasonably resistant to erosion.

Materials 1D (MX-89) and 2D (MX-2600) had the best resistance to erosion when compared to other materials laid up from 1/2- by 1/2-inch (1.27- by 1.27-cm) squares (see fig. 10(d)). The molding compounds were similar in erosion resistance to the 90° layup (compare figs. 10(c) and (d)). The molded squares actually approach a 90° to the centerline orientation (see fig. 6(d)) but are significantly less expensive than the tape layups.

All of the materials tested in the rosette configuration eroded at a very high rate. Figure 10(e) shows material 10E (quartz reinforcement) as being superior to all of the other materials tested with a rosette configuration.

The unexpectedly poor showing of some materials in erosion resistance, together with inconsistent results for various layup angles may have been due to inadequate quality control during component manufacturing. Although quartz-reinforced material was superior from a performance point of view, the MX-2600 material, number 2, was quite high in erosion resistance and char resistance and was the lowest cost material tested.

Char Performance of Ablative Nozzles

The average percent char-through of all nozzles tested has been compared with respect to the fabric orientation angle to the engine centerline. Figure 11(a) shows a curve of the average char-through at the throat plane and figure 11(b) shows the char at both the entrance and exit planes. All three curves have the same general shape. On each curve, the 1/2- by 1/2-inch (1.27- by 1.27-cm) squares and the rosette layup are entered at the measured char level. The 1/2- by 1/2-inch (1.27- by 1.27-cm) squares and the rosette layup appear to be equivalent in percent char-through to a 50° fabric orientation at the throat plane. The rosette layup for both the entrance and exit planes of the nozzle had the lowest percent char-through and is equivalent to a 0° fabric orientation if fabric orientation curves are extrapolated.

No apparent difference in the percent char-through was found for the 1/2- by 1/2-inch (1.27- by 1.27-cm) squares either in the entrance or exit plane of the nozzle. The same value was obtained regardless of nozzle location, indicating that the heat flux in these two areas was quite similar.

Since the effective fabric angle differs greatly from entrance to exit, it would seem to indicate that the primary method of charring at constant heat flux might be related to the length of the fabric heat path. The length of the heat path is determined by the angle formed between the internal surface contour of the nozzle and the fabric orientation regardless of the nozzle plane location. The average percent char can then be considered as a function of the fabric orientation angle to the gas flow as in figure 12. A sketch of the nozzle contour is included for clarity. The points shown are averages of all the available data. The curve suggests the desirability of maintaining a low angle of fabric orientation to the gas flow from a char standpoint. Combining minimum char orientation with erosion resistant orientation in the required areas of the nozzle should result in minimum engine weight. The rosette layup as fabricated acted as a 0° to gas flow orientation because the plies were laid up longitudinally and were radially compressed to effect an almost parallel layup to the gas flow.

SUMMARY OF RESULTS

An investigation was conducted to evaluate the erosion resistance and charring characteristics of ten silica-reinforced ablative materials and five fabric orientations as nozzle sections of a storable propellant (nitrogen-tetroxide and a 50-50 blend of unsymmetrical dimethylhydrazine and hydrazine) rocket engine. Testing was performed at an oxidant-to-fuel ratio of 1.6, chamber pressure of 100 psia (689 kN/m^2), a nominal throat diameter of 7.82 inches (19.8 cm), and a firing duration of 150 seconds. The results from the investigation are summarized as follows:

1. A quartz fabric with a 90° orientation angle impregnated with a polyimide resin was superior in erosion resistance to all other materials tested regardless of impregnating resin, filler, or fabric orientation.

2. A 60° fabric orientation was generally superior in throat erosion resistance to all other fabric orientations tested.

3. The depth of char and, therefore, engine weight can be minimized by preferential orientation of the fabric in the entrance and exit sections of the nozzle to effect angles approaching 0° to the gas flow.

4. The 0° helix angle used for all the rosette layup nozzles resulted in delaminations and severe erosion.

5. Careful attention to quality control of materials and processes are essential to provide consistent firing results.

6. The lowest cost material tested, MX-2600, had high resistance to erosion and relatively low char rates.

CONCLUDING REMARKS

The design of an ablative rocket chamber requires resistance to erosion at the throat to meet thrust level and misalinement specificiations. However, the nozzle entrance and exit, where erosion is minimal, require attention to char depth to minimize engine weight. Results of this report show that the optimum erosion and char resistance occur at widely different fabric orientations. Fabric orientation angles to the gas flow near zero produce the lowest amount of char-through but tend to delaminate in high shear fields such as the throat region. On the other hand, a 60° orientation produced the best erosion resistance but was somewhat higher in charring. The resulting implication is that the best use of ablative reinforcements in a rocket engine would be to use a relatively flat layup angle at the entrance and the exit with a 60° orientation at the throat. This combination would produce the maximum erosion resistance at the throat and minimum wall thicknesses at the entrance and exit sections of the nozzle.

REFERENCES

1. Peterson, Donald A.: Experimental Evaluation of High-Purity-Silica Reinforced Ablative Composites as Nozzle Sections of 7.8-Inch (19.8-cm) Diameter Throat Storable-Propellant Rocket Engine. NASA TM X-1391, 1967.

2. Shinn, Arthur M., Jr.: Experimental Evaluation of Six Ablative-Material Thrust Chambers as Components of Storable-Propellant Rocket Engines. NASA TN D-3945, 1967.

3. Pavli, A. J.: Experimental Evaluation of Several Advanced Ablative Materials as Nozzle Sections of a Storable-Propellant Rocket Engine. NASA TM X-1559, 1968.

TABLE I. - MATERIALS

Nozzle	Material		Fabric orientation	Throat radius change after 150-second firing		Average char through at throat plane, percent
	Composition	Supplier's designation (a)		mil	mm	
1A	70-percent high silicon dioxide - 30-percent phenolic	MX-89	30° centerline	190	4.82	48
1B			60° centerline	165	4.19	52
1C			90° centerline	180	4.57	60
1D			1/2- by 1/2-inch (1.27- by 1.27-cm) square	175	4.44	52
1E			Rosette	235	5.97	51.2
2A	61-percent high silicon dioxide - 29-percent phenolic - silicon di-oxide filler	MX-2600	30° centerline	[b]145	3.68	44
2B			60° centerline	150	3.81	53.5
2C			90° centerline	205	5.22	61.5
2D			1/2- by 1/2-inch (1.27- by 1.27-cm) square	190	4.82	60
3A	62-percent high silicon dioxide - 32-percent polyamide modified phenolic	MX-19	30° centerline	[b]165	4.19	44
3B			60° centerline	140	3.56	48
3C			90° centerline	250	6.35	57.5
3D			1/2- by 1/2-inch (1.27- by 1.27-cm) square	220	5.59	44
4A	80-percent high silicon dioxide - 20-percent polyamide modified phenolic	MX-87	30° centerline	[b]205	5.22	36.6
4B			60° centerline	220	5.59	52
4C			90° centerline	205	5.22	50.5
4D			1/2- by 1/2-inch (1.27- by 1.27-cm) square	215	5.46	44
4E			Rosette	[b]330	8.38	45.5
5A	67-percent silicon di-oxide - 3-percent chrome salt - 30 per-cent phenolic	MXS 141	30° centerline	250	6.35	47.2
5B			60° centerline	240	6.10	52.0
5C			90° centerline	245	6.23	56.0
5D			1/2- by 1/2-inch (1.27- by 1.27-cm) square	245	6.23	48.8
5E			Rosette	315	8.00	48.0
6A	70-percent high silicon dioxide - 30-percent modified phenolic	4S-4161	30° centerline	200	5.08	42.5
6B			60° centerline	175	4.44	52.0
6C			90° centerline	190	4.82	53.6
6D			1/2- by 1/2-inch (1.27- by 1.27-cm) square	185	4.70	48.8
7A	60-percent high silicon dioxide - 40-percent elastomeric phenyl silane	FM-201S	30° centerline	[b]225	5.72	44.0
7B			60° centerline	225	5.72	51.0
7C			90° centerline	255	6.47	53.5
7E			Rosette	[b,c]450	11.4	52.0
8B	70-percent high silicon dioxide - 30-percent high-temperature phenolic	MXS-115	60° centerline	200	5.08	60
8C			90° centerline	250	6.35	64
9C	70-percent quartz - 30-percent polyimide	--------	90° centerline	130	3.30	64
10E	70-percent quartz - 30-percent phenolic	MX-5091	Rosette	220	5.59	54

[a] All nozzles fabricated by Edler Industries.
[b] Fabric delamination.
[c] After 110-sec firing.

15

TABLE II. - FIRING RESULTS - DECREASING EROSION RESISTANCE

Throat radius change		Char through at throat plane, percent	Nozzle	Throat radius change		Char through at throat plane, percent	Nozzle
mil	mm			mil	mm		
130	3.30	63.0	9C	215	5.46	44.0	4D
140	3.56	48.0	3B	220	5.59	44.0	3D
[a]145	3.68	44.0	2A	220	5.59	52.0	4B
150	3.81	53.5	2B	220	5.59	54.0	10E
165	4.19	52.0	1B	[a]225	5.72	44.0	7A
[a]165	4.19	44.0	3A	225	5.72	51.0	7B
175	4.44	52.0	6B	235	5.97	51.2	1E
175	4.44	52.0	1D	240	6.10	52.0	5B
180	4.57	60.0	1C	245	6.23	56.0	5C
185	4.72	48.8	6D	245	6.23	48.8	5D
190	4.82	48.0	1A	250	6.35	57.5	3C
190	4.82	60.0	2D	250	6.35	47.2	5A
190	4.82	53.6	6C	250	6.35	64.0	8C
200	5.08	60.0	8B	255	6.47	53.5	7C
[a]200	5.08	42.0	6A	315	8.00	48.0	5E
205	5.22	61.5	2C	330	8.38	45.5	4E
[a]205	5.22	36.6	4A	[a,b]450	11.4	52.0	7E
205	5.22	50.5	4C				

[a]Fabric delamination.
[b]After 110-sec firing.
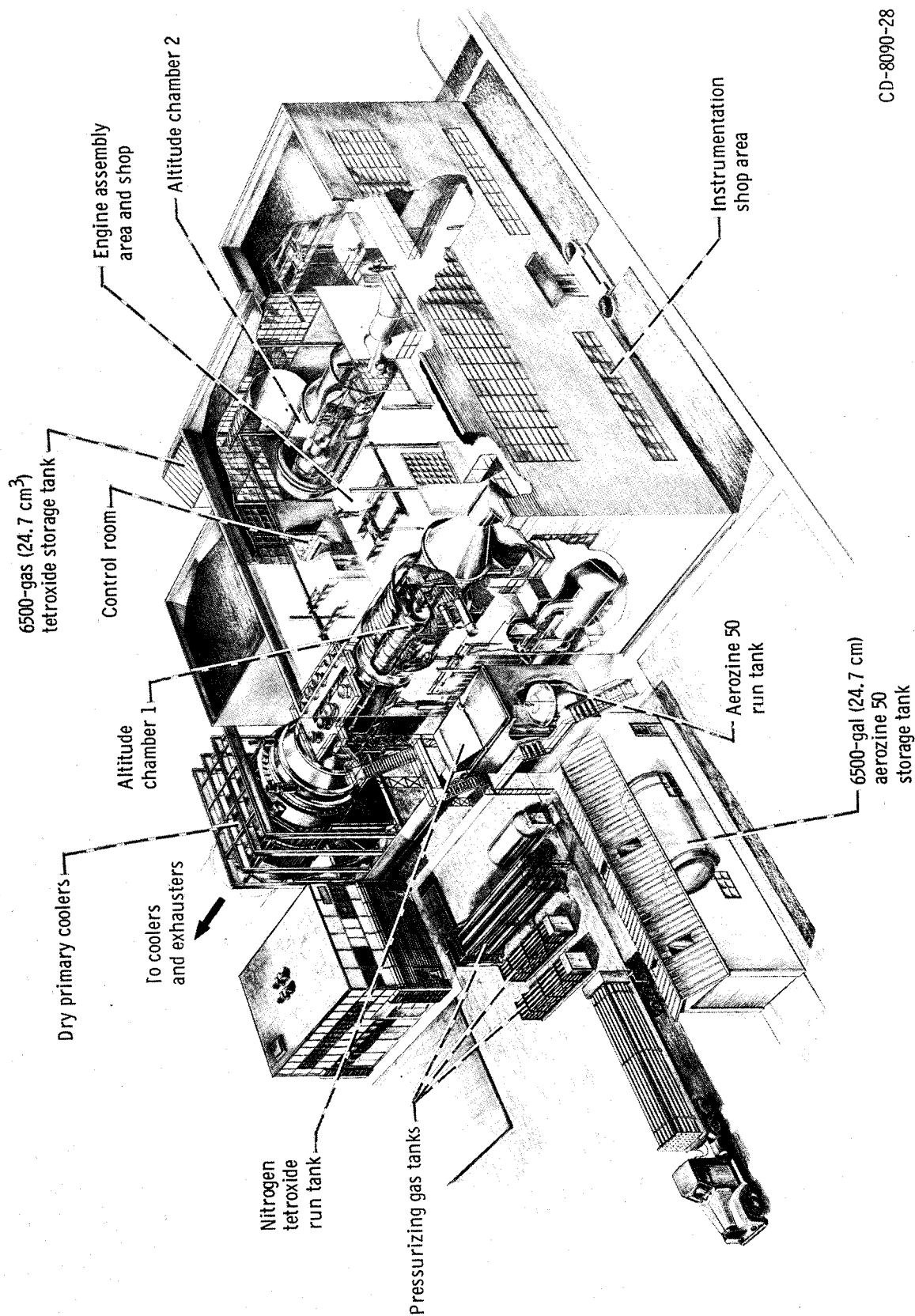
Figure 1. – Altitude facility.

Engine assembly area and shop

Altitude chamber 2

6500-gas (24.7 cm³) tetroxide storage tank

Control room

Altitude chamber 1

Dry primary coolers

To coolers and exhausters

Nitrogen tetroxide run tank

Pressurizing gas tanks

Instrumentation shop area

Aerozine 50 run tank

6500-gal (24.7 cm) aerozine 50 storage tank

CD-8090-28

17
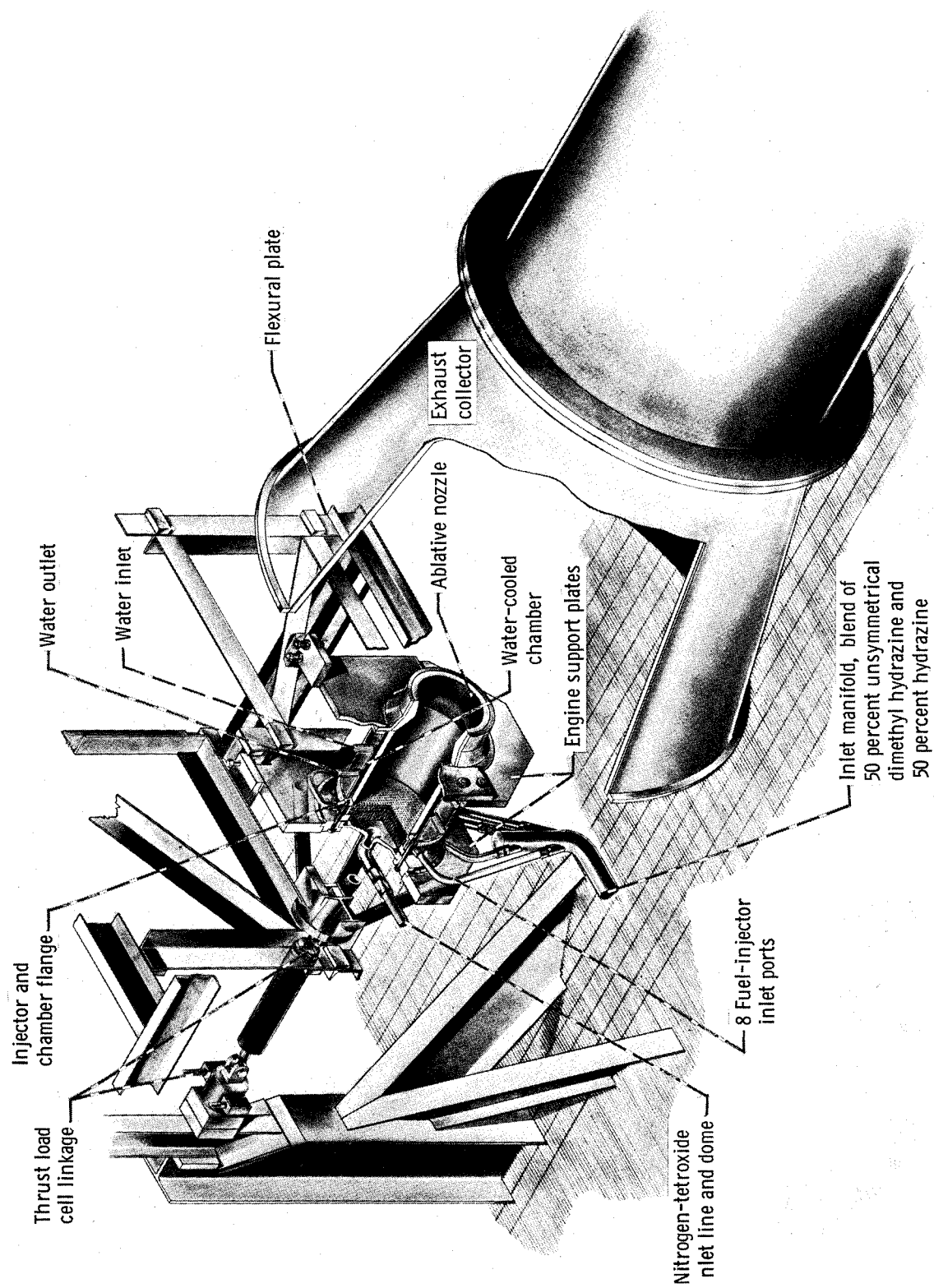
Figure 2. – Cutaway view of test chamber and injector assembly.

CD-9006-28

Injector-face
chamber-
pressure tap

Injector-face
chamber-
pressure tap

C-65-1808

Face plate pattern

Fan

Converging angle

C-65-1804
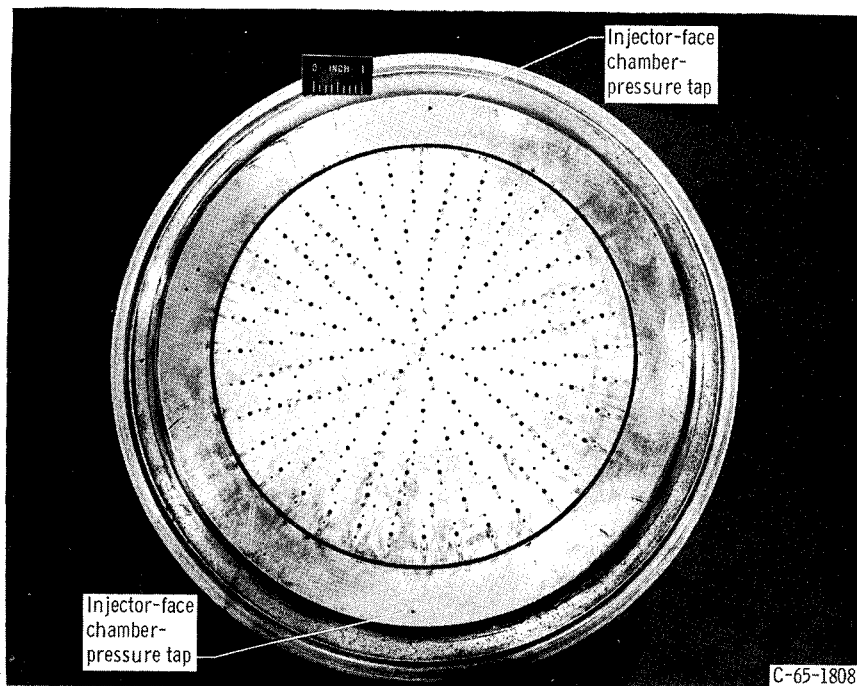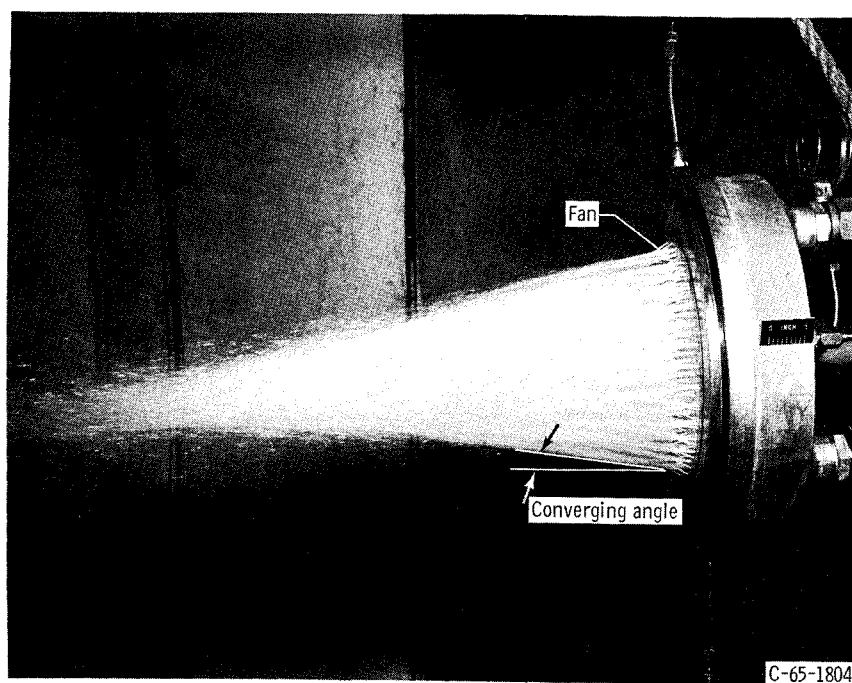
Water-flow test.

Figure 3. – Injector.

Water inlets (4) **Water outlets (4)**

11.280 (28.6) diam,
0.003 to 0.005 (0.00762 to 0.0127)
clearance for brazing

45 Equally
spaced ribs

0.13 (0.33)

0.12
(0.304)

2.50
(6.35 cm)

7° 30'

Section A-A

10.78
(27.4)

7.82
(19,8)

5.44 (13.8)   20.00 (50.8)
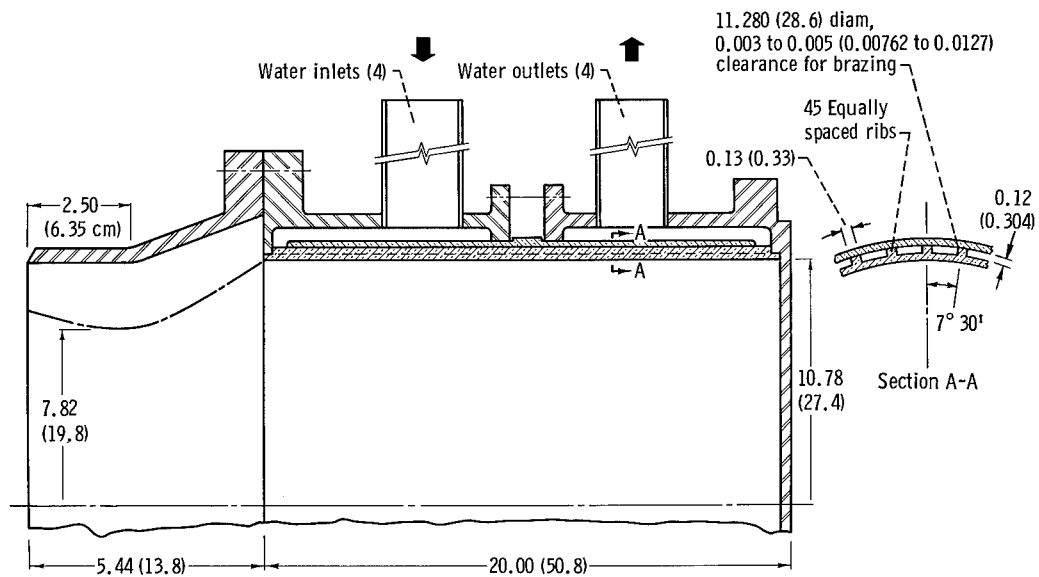
CD-9007-28

Figure 4. – Water-cooled combustion chamber and nozzle assembly. All linear dimensions are in inches (cm).)

2.92 (7.42)

Diam
12.890 (32.7)
12.39 (31.4)

Asbestos phenolic
flat wrap

20°

Diam

2.28 (5.8) rad

10.765 (27.3)
10.26 (26.1)

10.70 (27.2)

Ablative
material

8.80 (22.3)

15°

30°

Throat diam,
7.82 (19.8)

5.44 (13.8)

Gas flow
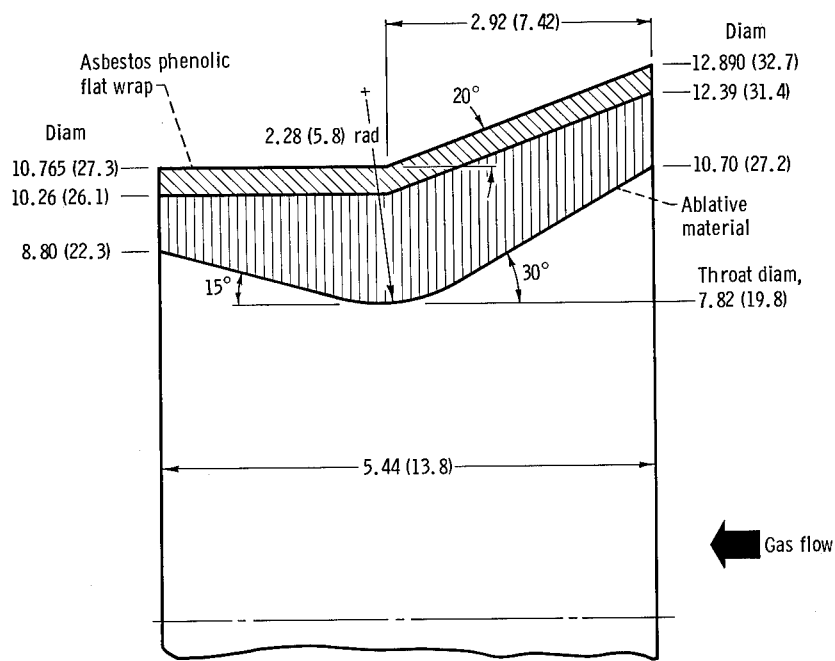
CD-9008-28

Figure 5. – Ablative nozzle. All linear dimensions are in inches (cm).)

Gas flow
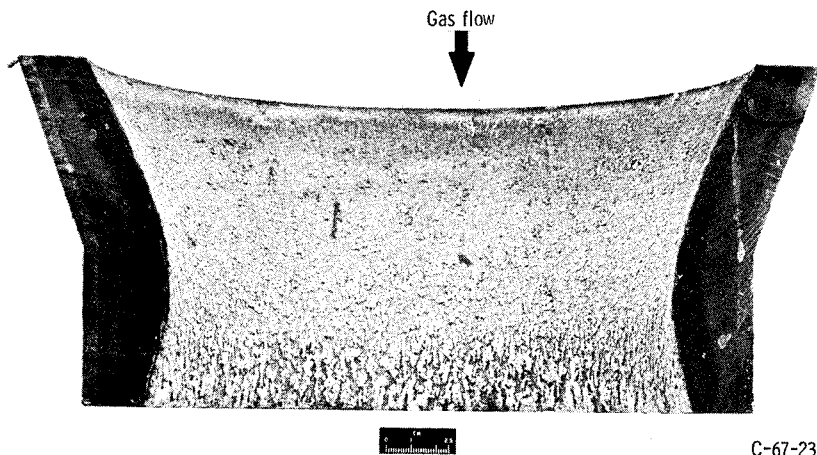
C-67-237

(a) Nozzle 1A; orientation, 30° centerline; 70-percent silicon dioxide - 30-percent phenolic.
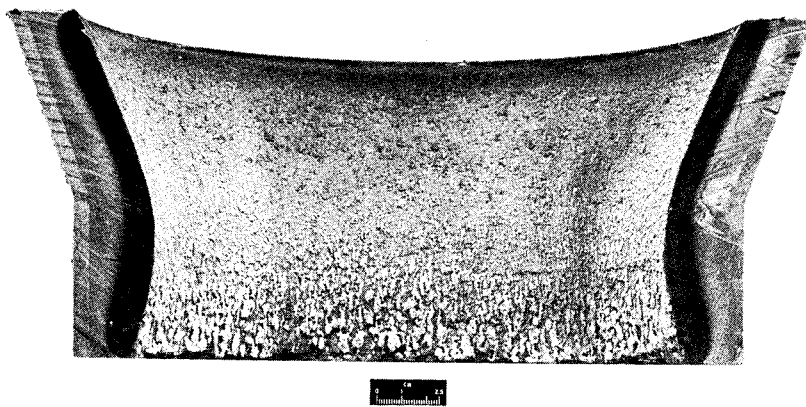
C-67-236

(b) Nozzle 1B; orientation, 60° centerline; 70-percent silicon dioxide - 30-percent phenolic.
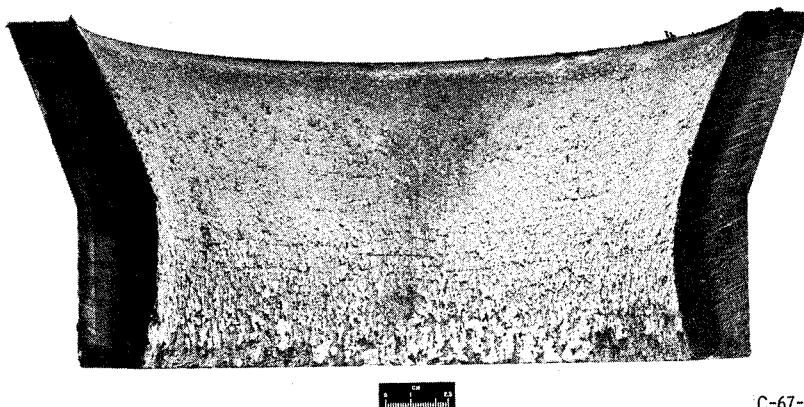
C-67-235

(c) Nozzle 1C; orientation, 90° centerline; 70-percent silicon dioxide - 30-percent phenolic.

Figure 6. - Post-test photographs.
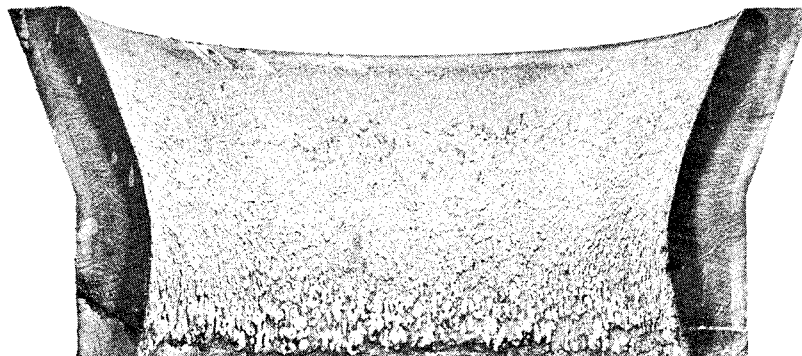
C-67-234

(d) Nozzle 1D; orientation, 1/2 by 1/2 square; 70-percent silicon dioxide - 30-percent phenolic.
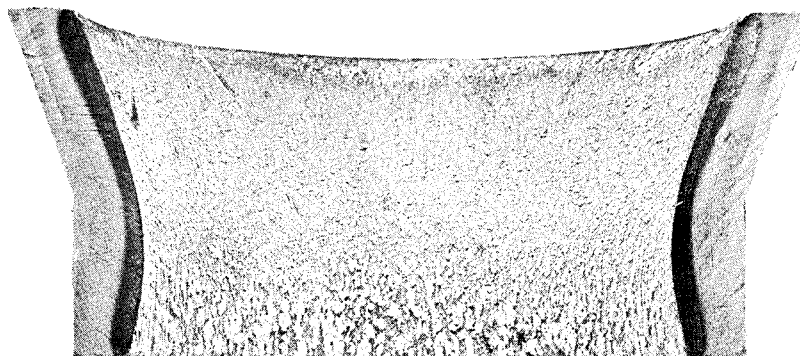
C-67-233

(e) Nozzle 1E; orientation, rosette; 70-percent silicon dioxide - 30-percent phenolic.
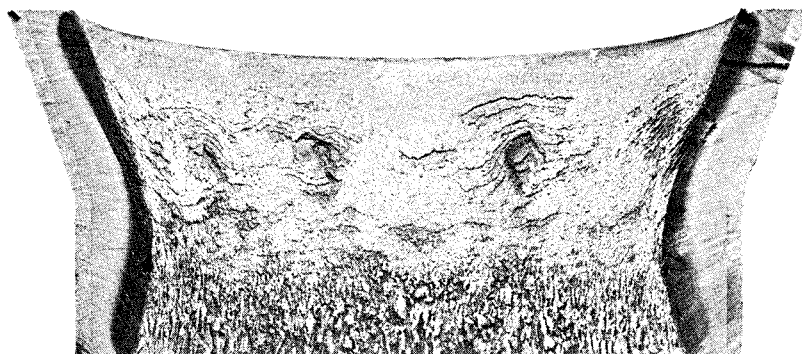
C-67-232

(f) Nozzle 2A; orientation, 30° centerline; 61-percent silicon dioxide - 31-percent phenolic - 8-percent silicon dioxide filler.

Figure 6. - Continued.
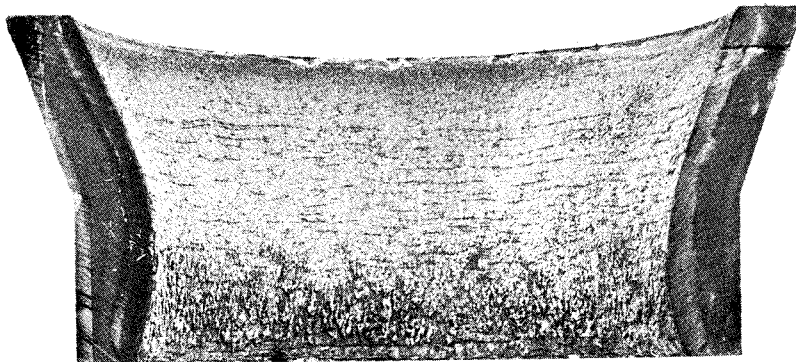
C-67-231

(g) Nozzle 2B; orientation 60° centerline; 61-percent silicon dioxide - 31-percent phenolic - 8-percent silicon dioxide filler.
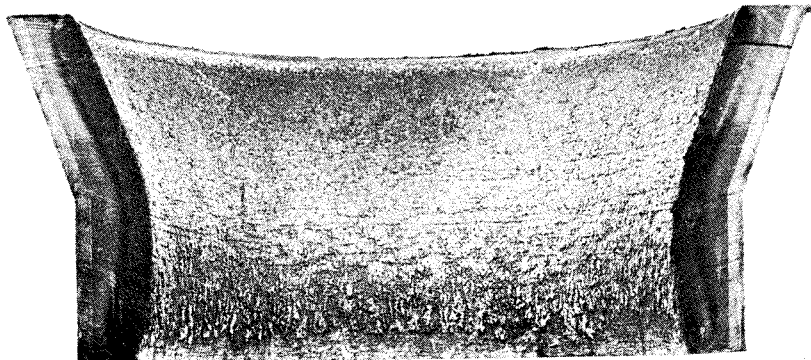
C-67-230

(h) Nozzle 2C; orientation 90° centerline; 61-percent silicon dioxide - 31-percent phenolic - 8-percent silicon dioxide filler.
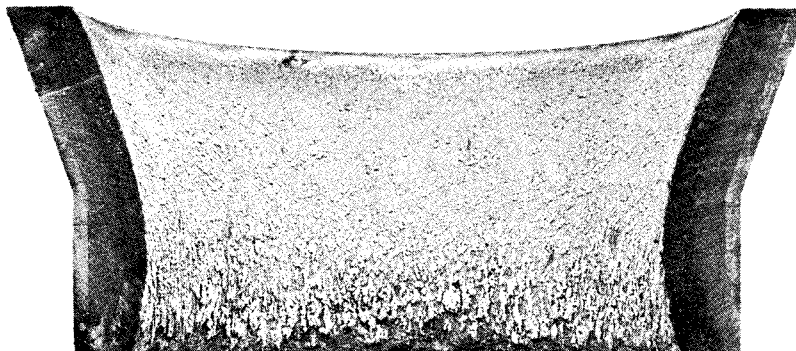
C-67-229

(i) Nozzle 2D; orientation, 1/2 by 1/2 square; 61-percent silicon dioxide - 31-percent phenolic - 8-percent silicon dioxide filler.

Figure 6. - Continued.
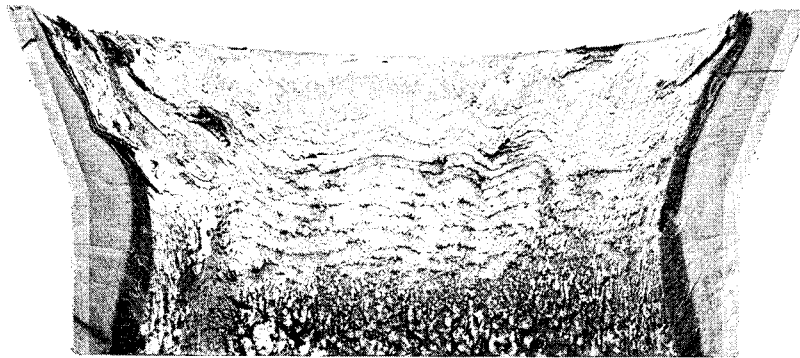
C-67-228

(j) Nozzle 3A; orientation, 30° centerline; 68-percent silicon dioxide - 32-percent phenolic polyamide.
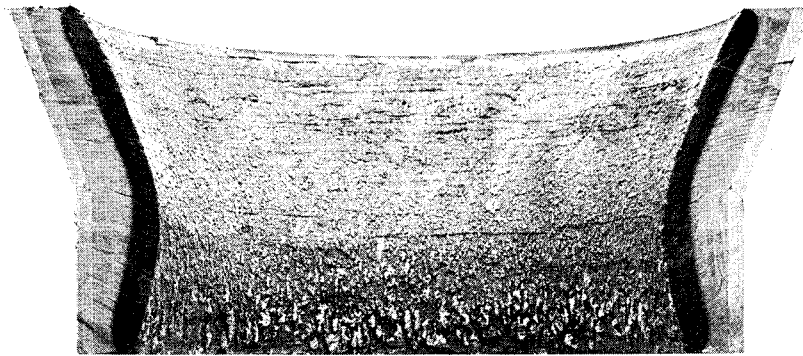
C-67-227

(k) Nozzle 3B; orientation, 60° centerline; 68-percent silicon dioxide - 32-percent phenolic polyamide.
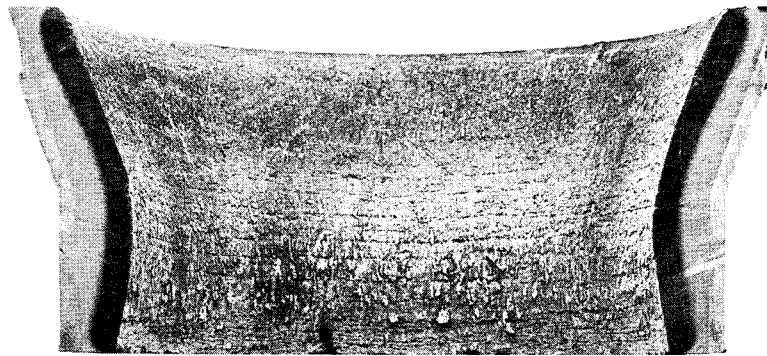
C-67-226

(l) Nozzle 3C; orientation, 90° centerline; 68-percent silicon dioxide - 32-percent phenolic polyamide.

Figure 6. - Continued.
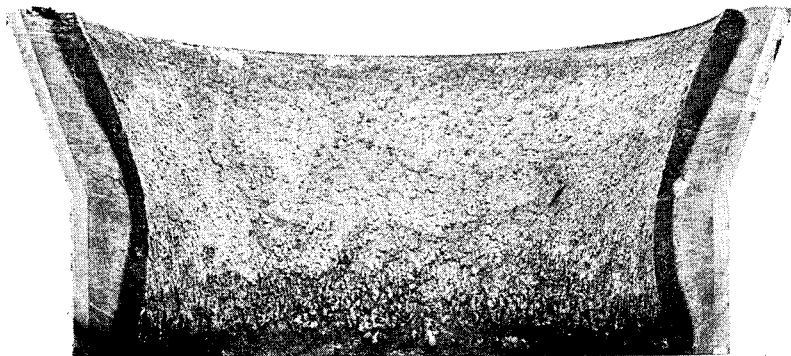
C-67-225

(m) Nozzle 3D; orientation, 1/2 by 1/2 square; 68-percent silicon dioxide - 32-percent phenolic polyamide.
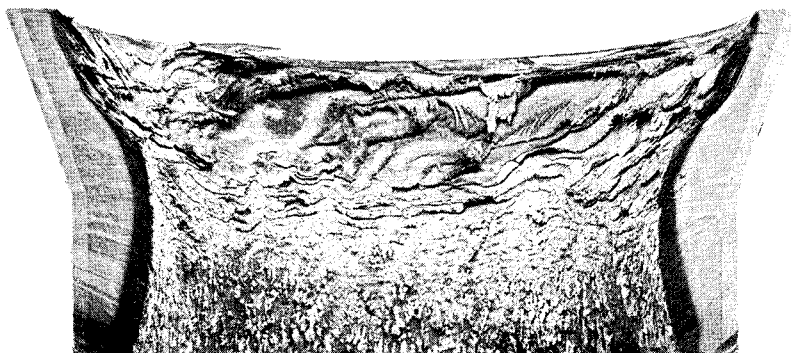
C-67-224

(n) Nozzle 4A; orientation, 30° centerline; 80-percent silicon dioxide - 20-percent phenolic polyamide.

C-67-223

(o) Nozzle 4B; orientation, 60° centerline; 80-percent silicon dioxide - 20-percent phenolic polyamide.

Figure 6. - Continued.

25
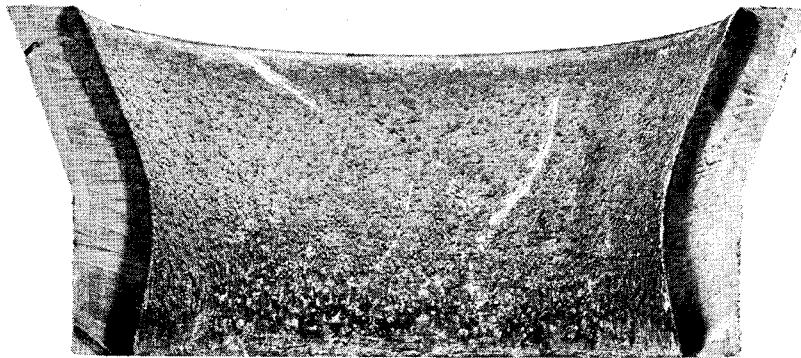
C-67-222

(p) Nozzle 4C; orientation, 90° centerline; 80-percent silicon dioxide - 20-percent phenolic polyamide.
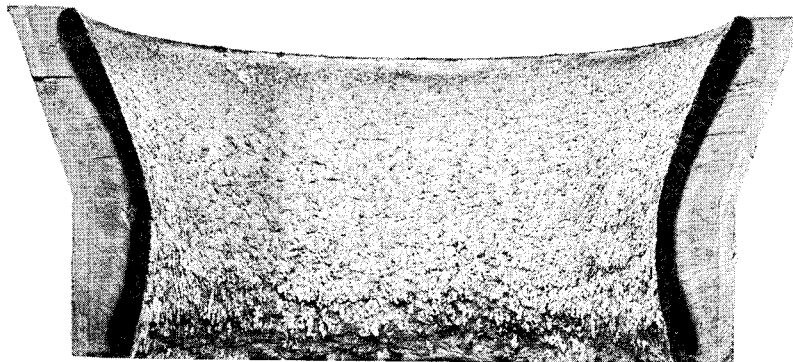
C-67-221

(q) Nozzle 4D; orientation, 1/2 by 1/2 square; 80-percent silicon dioxide - 20-percent phenolic polyamide.

C-67-220

(r) Nozzle 4E; orientation, rosette; 80-percent silicon dioxide - 20-percent phenolic polyamide.

Figure 6. - Continued.
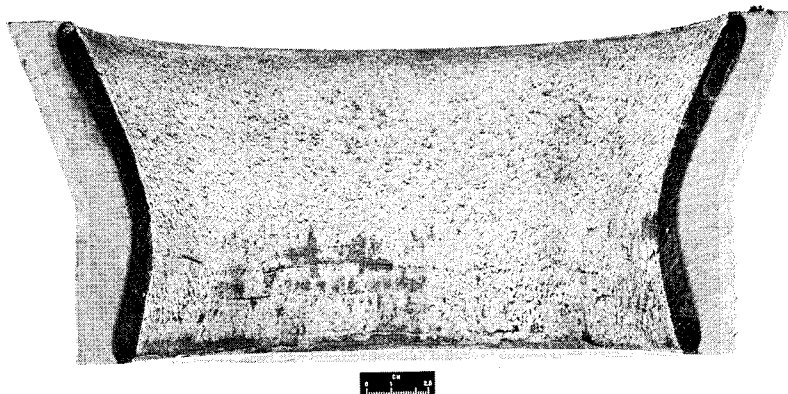
C-66-4412

(s) Nozzle 5A; orientation, 30° centerline; 67-percent silicon dioxide - 3 percent chrome sale -
30-percent phenolic.
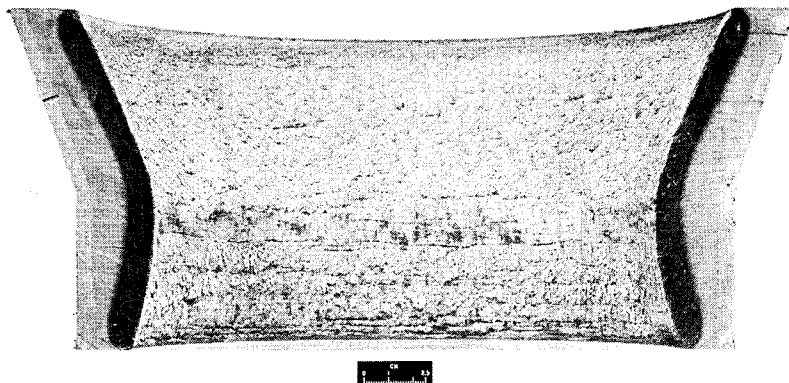
C-66-4413

(t) Nozzle 5B; orientation, 60° centerline; 67-percent silicon dioxide - 3-percent chrome salt -
30-percent phenolic.
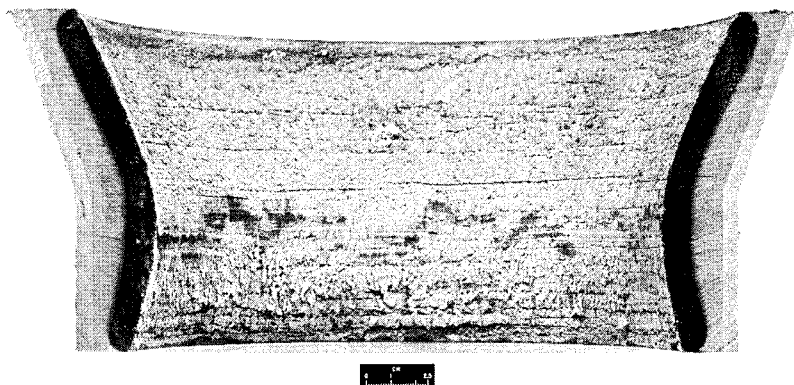
-66-4414

(u) Nozzle 5C; orientation, 90° centerline; 67-percent silicon dioxide - 3-percent chrome salt -
30-percent phenolic.

Figure 6. - Continued.
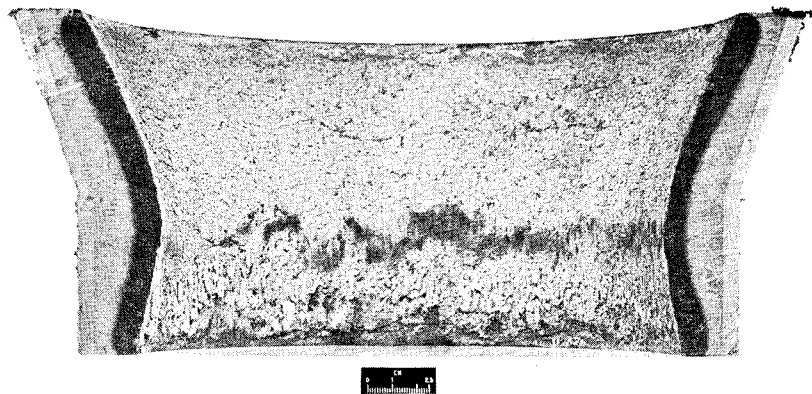
C-66-4416

(v) Nozzle 5D; orientation, 1/2 by 1/2 square; 67-percent silicon dioxide - 3-percent chrome salt - 30-percent phenolic.
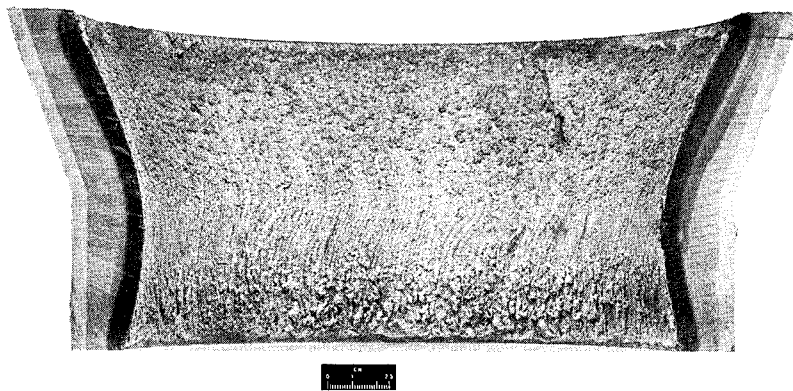
C-66-4415

(w) Nozzle 5E; orientation, rosette; 67-percent silicon dioxide - 3-percent chrome salt - 30-percent phenolic.
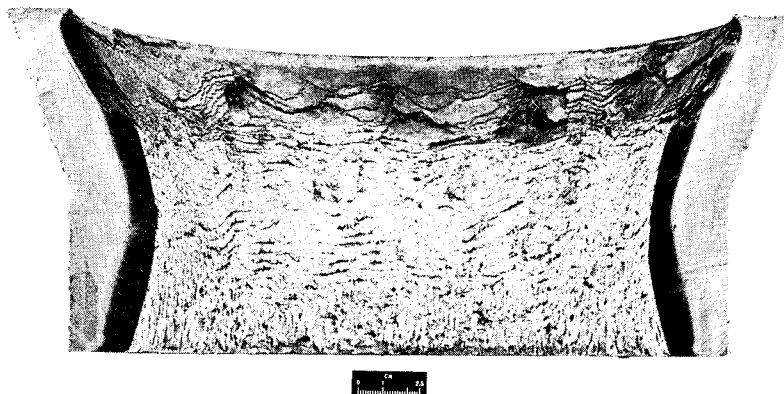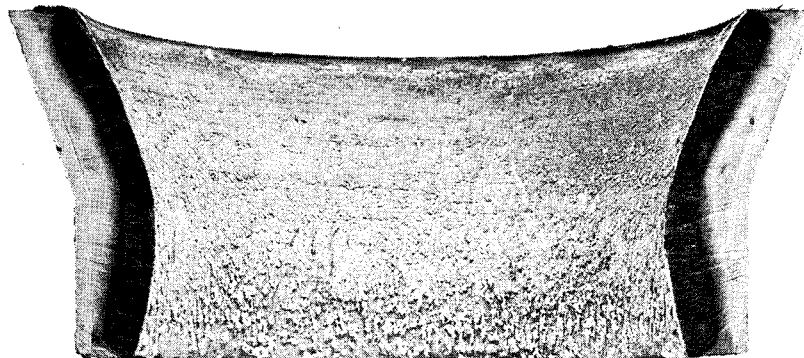

C-66-4573

(x) Nozzle 6A; orientation, 30° centerline; 70-percent silicon dioxide - 30-percent modified phenolic.
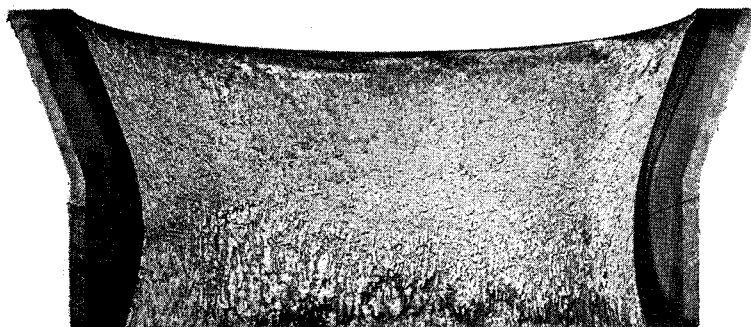
Figure 6. - Continued.

C-66-4574

(y) Nozzle 6B; orientation 60° centerline; 70-percent silicon dioxide - 30-percent modified phenolic.
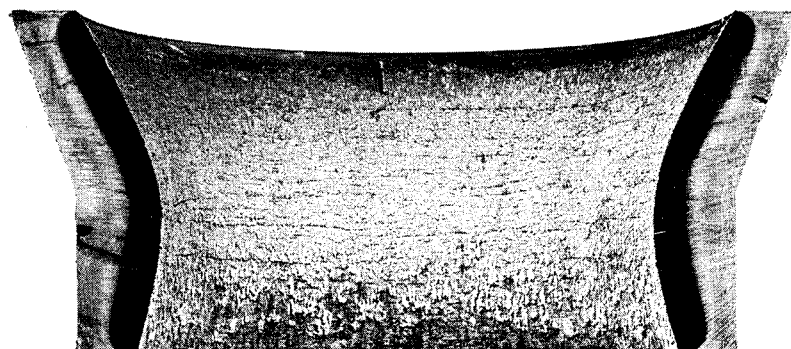
C-66-4575

(z) Nozzle 6C; orientation, 90° centerline; 70-percent silicon dioxide - 30-percent modified phenolic.
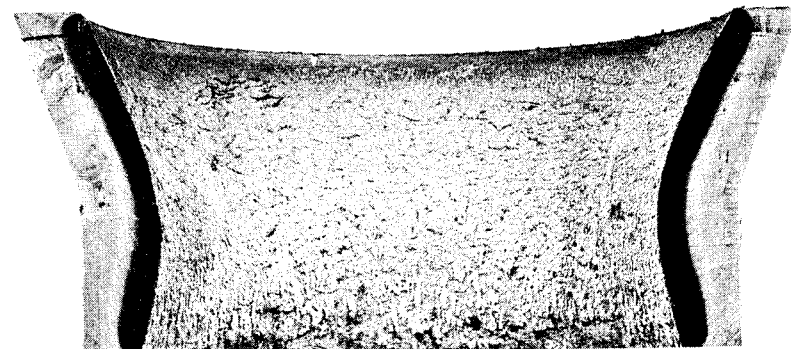
C-66-4576

(aa) Nozzle 6D; orientation, 1/2 by 1/2 square; 70-percent silicon dioxide - 30-percent modified phenolic.

Figure 6. - Continued.

29

C-66-4421

(bb) Nozzle 7A; orientation, 30° centerline; 60-percent silicon dioxide - 40-percent elastomeric phenyl silane.
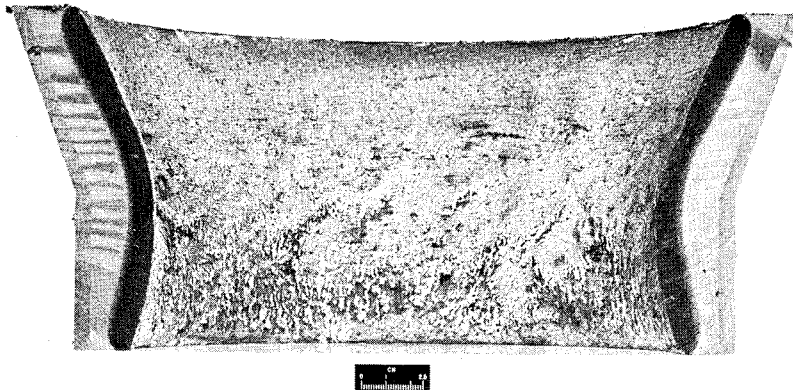
C-66-4422

(cc) Nozzle 7B; orientation, 60° centerline; 60-percent silicon dioxide - 40-percent elastomeric phenyl silane.
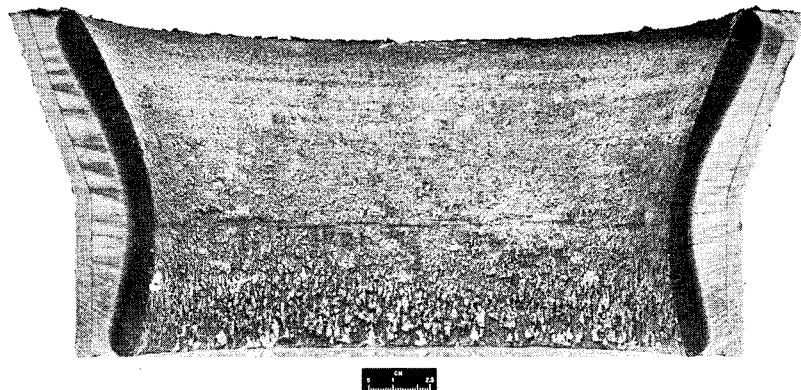
C-66-4423

(dd) Nozzle 7C; orientation, 90° centerline; 60-percent silicon dioxide - 40-percent elastomeric phenyl silane.

Figure 6. - Continued.
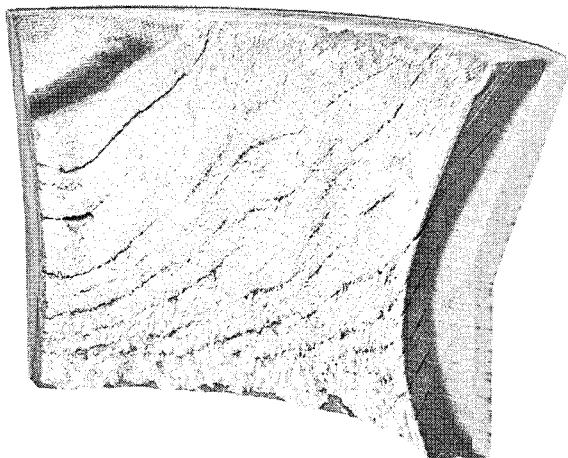
C-68-1278

Rosette orientation from ref. 1.

C-66-4424

(ee) Nozzle 7E; orientation, rosette; 60-percent silicon dioxide - 40-percent elastomeric phenyl silane.
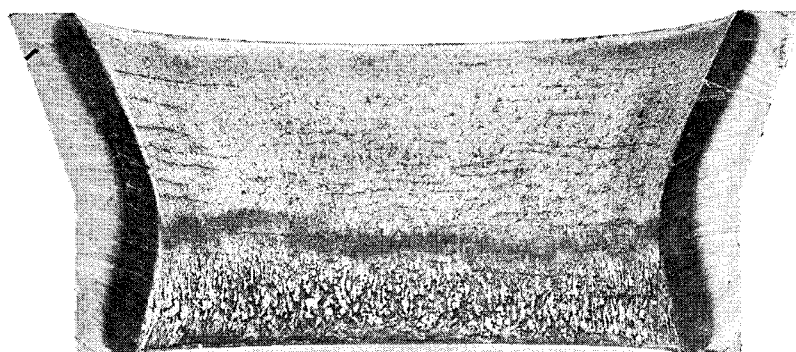
C-66-4418

(ff) Nozzle 8B; orientation, 60° centerline; 70-percent silicon dioxide - 30-percent high-temperature phenolic.

Figure 6. - Continued.
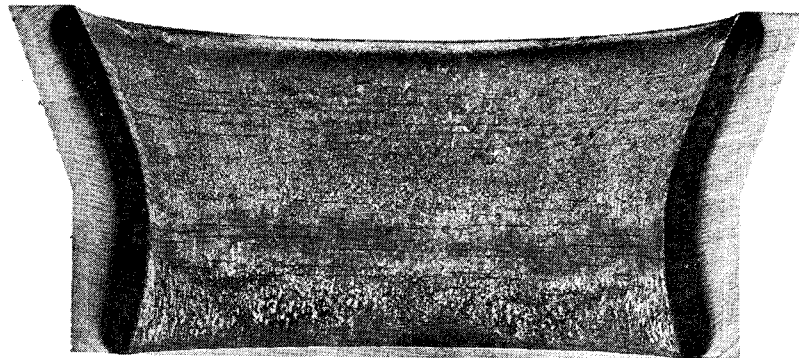
C-66-4420

(gg) Nozzle 8C; orientation, 90° centerline; 70-percent silicon dioxide - 30-percent high-temperature phenolic.

C-67-215

(hh) Nozzle 9C; orientation, 90° centerline; 70-percent silicon dioxide (quartz) - 30-percent polyimide.

C-67-2393

(ii) Nozzle 10E; orientation, rosette; 70-percent silicon dioxide (quartz) - 30-percent phenolic.

Figure 6. - Concluded.

Total throat radius change, in.

.24 .20 .16 .12 .08 .04 0

Total throat radius change, cm

.6 .5 .4 .3 .2 .1 0

Nozzle orientation

| 1A 30° | 1B 60° | 1C 90° | 1D 1/2 by 1/2 | 1E Rosette |

(a) Material 1, 70-percent silicon dioxide - 30-percent phenolic.

Delaminated

Total throat radius change, in.

.24 .20 .16 .12 .08 .04 0

Total throat radius change, cm

.6 .5 .4 .3 .2 .1 0

Nozzle orientation

| 2A 30° | 2B 60° | 2C 90° | 2D 1/2 by 1/2 |

(b) Material 2, 61-percent silicon dioxide - 31-percent phenolic - 8-percent silicon dioxide filler.

Figure 8. – Erosion as function of fabric orientation.

Throat radius change, in.

.28 .24 .20 .16 .12 .08 .04 0

Throat radius change, cm

.7 .6 .5 .4 .3 .2 .1 0 -.1

Throat area change, percent

14 12 10 8 6 4 2 0

Total firing time, sec

0 20 40 60 80 100 120 140 160

Figure 7. – Typical throat erosion curve. Nozzle 6B; orientation, 60° centerline; material, 70-percent silicon dioxide - 30-percent modified phenolic. Crosshatched area shows data spread for all nozzles tested except those that delaminated.
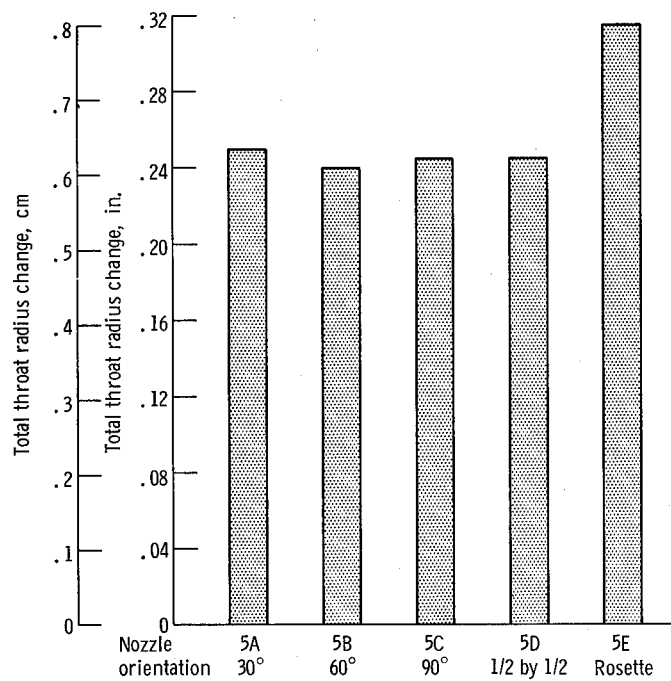
33

(c) Material 3, 68-percent silicon dioxide -
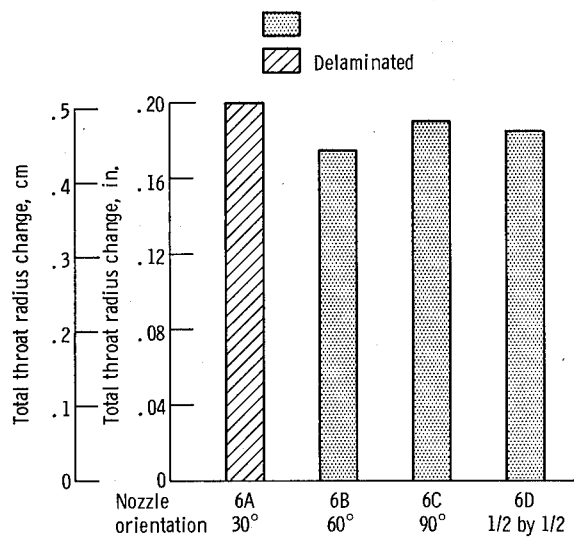32-percent phenolic polyamide.
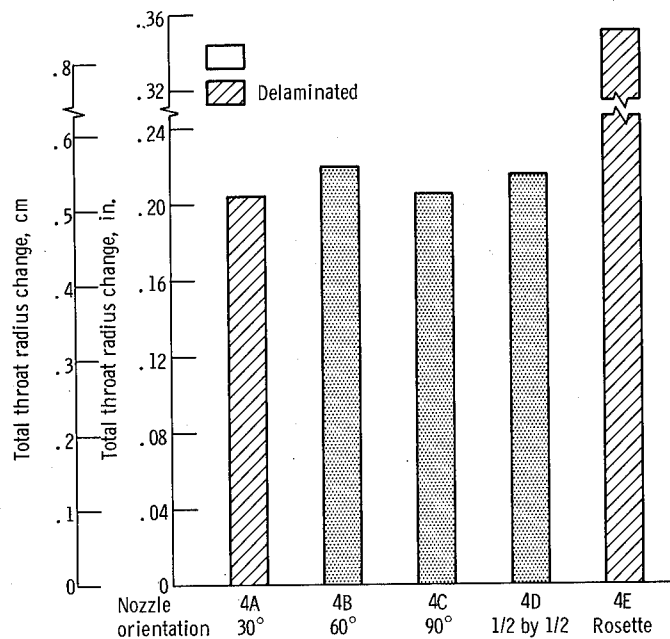
(d) Material 4, 80-percent silicon dioxide - 20-percent
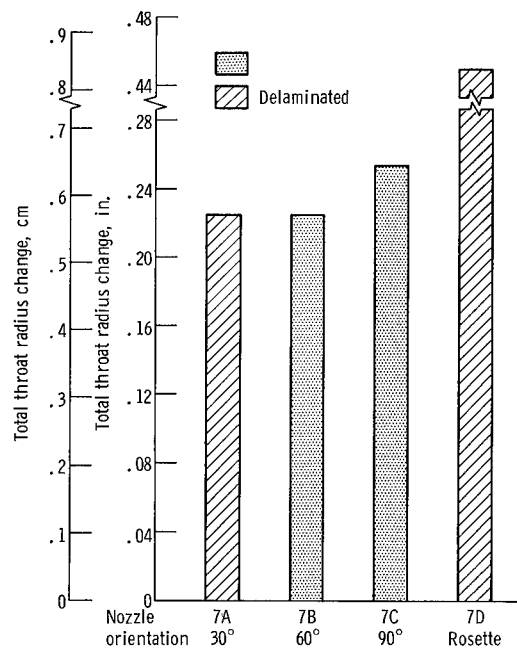phenolic polyamide.

Figure 8. - Continued.

34

(e) Material 5, 67-percent silicon dioxide – 3-percent chrome salt – 30-percent phenolic.
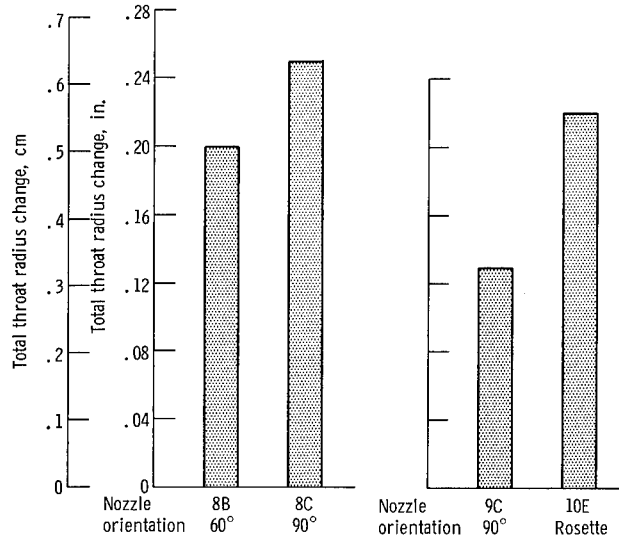

(f) Material 6, 70-percent silicon dioxide – 30-percent modified phenolic.

Figure 8. – Continued.

(g) Material 7, 60-percent silicon dioxide – 40-percent elastomeric phenyl silane.

(h) Material 8, 70-percent silicon dioxide – 30-percent high-temperature phenolic.

(i) Material 9, 70-percent quartz – 30-percent polyimide resin. Material 10, 70-percent quartz – 30-percent phenolic resin.
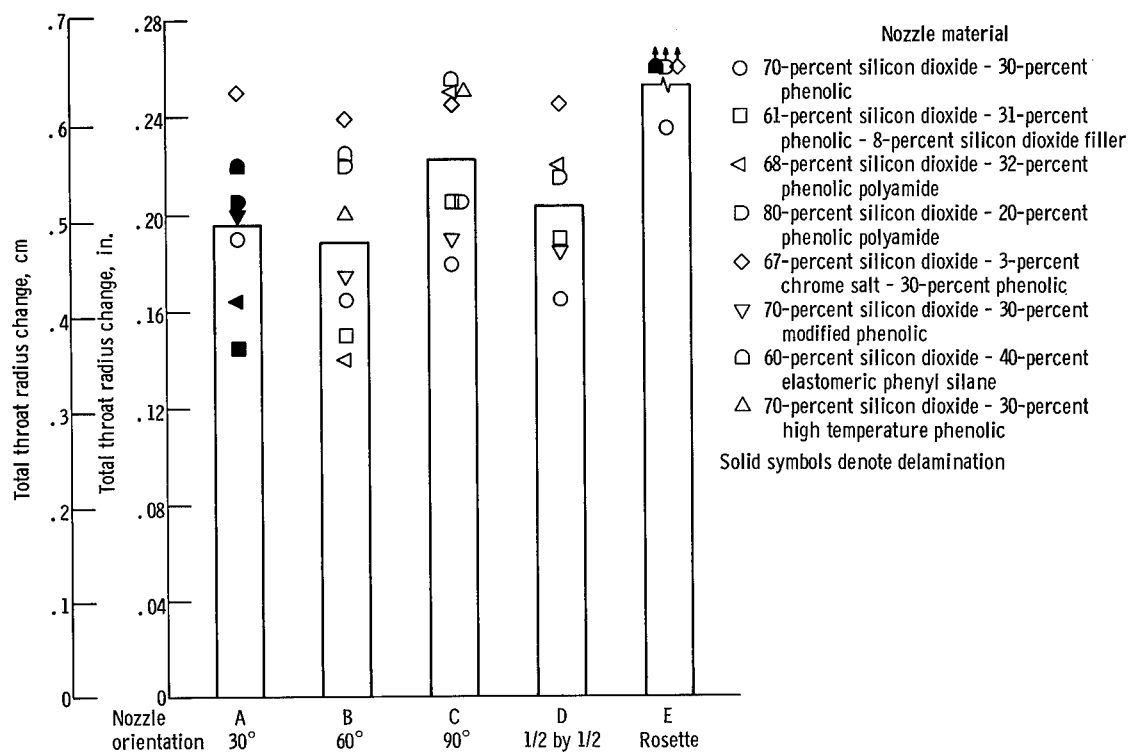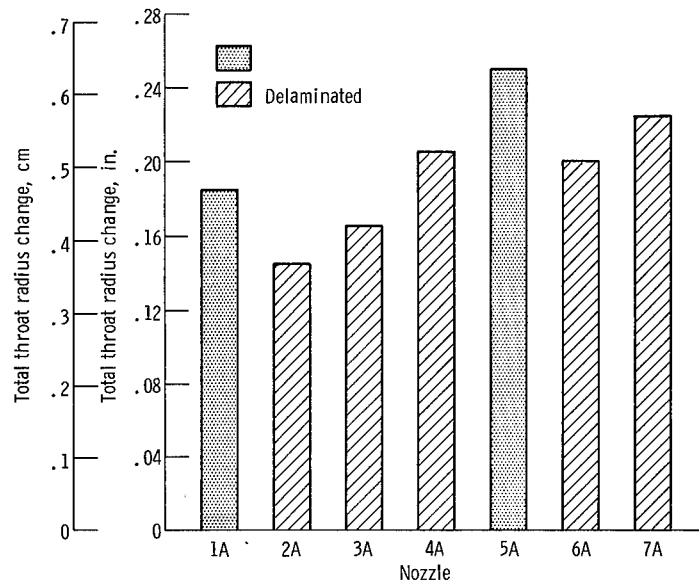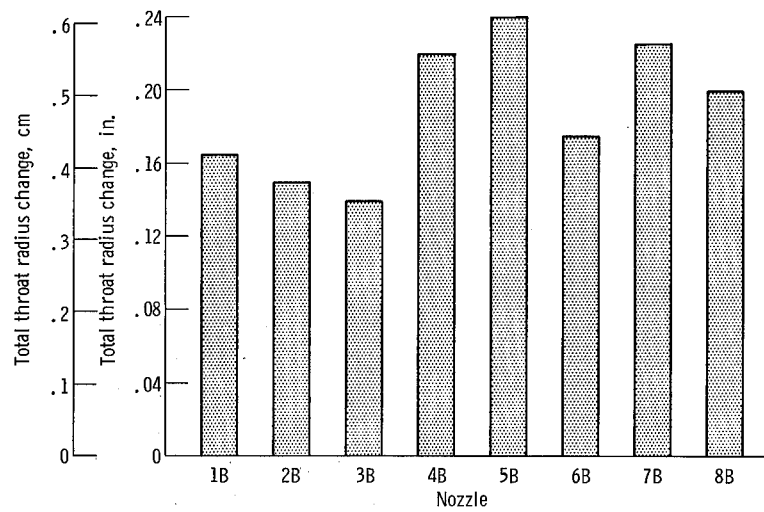
Figure 8. – Concluded.

Figure 9. - Average erosion of nozzle materials as function of fabric orientation.
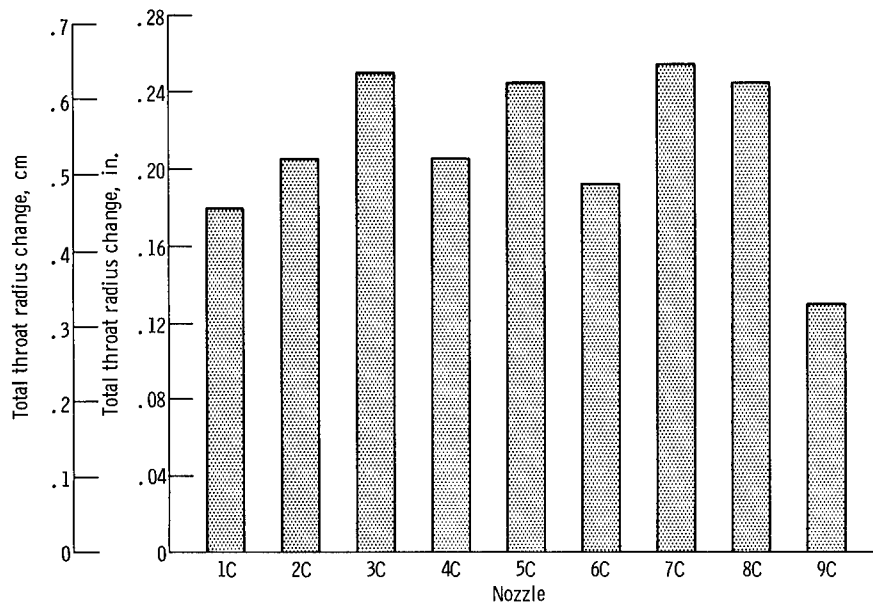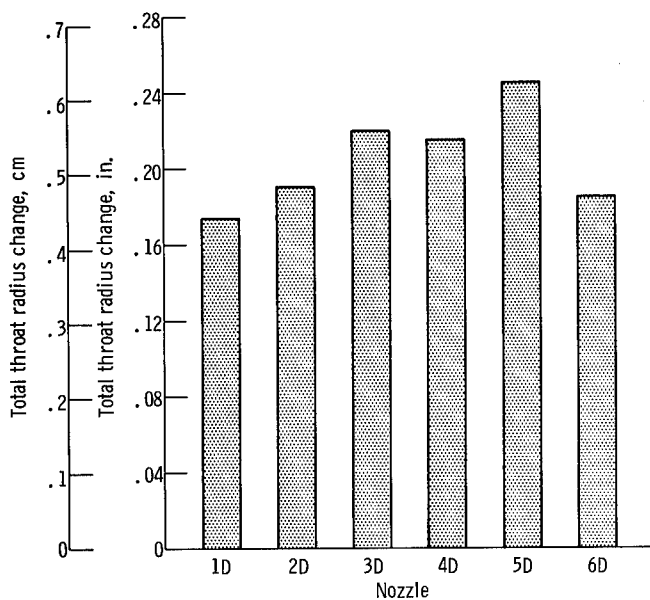
(a) Orientation, 30° centerline.
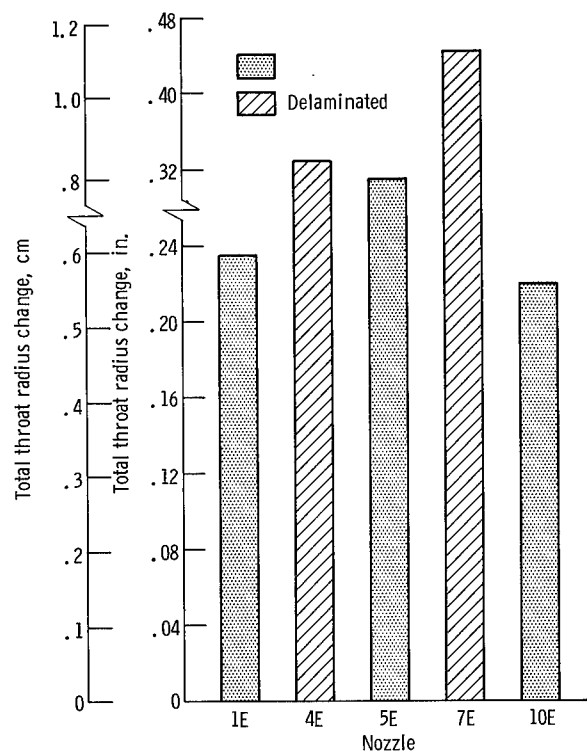
(b) Orientation 60° centerline.

Figure 10. – Effect of material orientation on erosion.

(c) Orientation, 90° centerline.

(d) Orientation, 1/2 by 1/2 square.

(e) Orientation, rosette.

Figure 10. – Concluded.

Orientation   Material

                         1   2   3   4   5   6   7   8   9   10

O 30° centerline   MX-89 MX-2600 MX-19 MX-87 MXS-141 4S-4161 FM 2015
□ 60° centerline   MX-89 MX-2600 MX-19 MX-87 MXS-141 4S-4161 FM 2015 MXS-115
◇ 90° centerline   MX-89 MX-2600 MX-19 MX-87 MXS-141 4S-4161 FM 2015 MXS-115 Quartz,
                                                                                   polyimide

△ 1/2 by 1/2 square MX-89 MX-2600 MX-19 MX-87 MXS-141   FM 2015
▽ Rosette   MX-89   MX-87 MXS-141 4S-4161   MX-5091

Solid symbols denote measured char levels

(a) Throat plane.   (b) Entrance and exit.
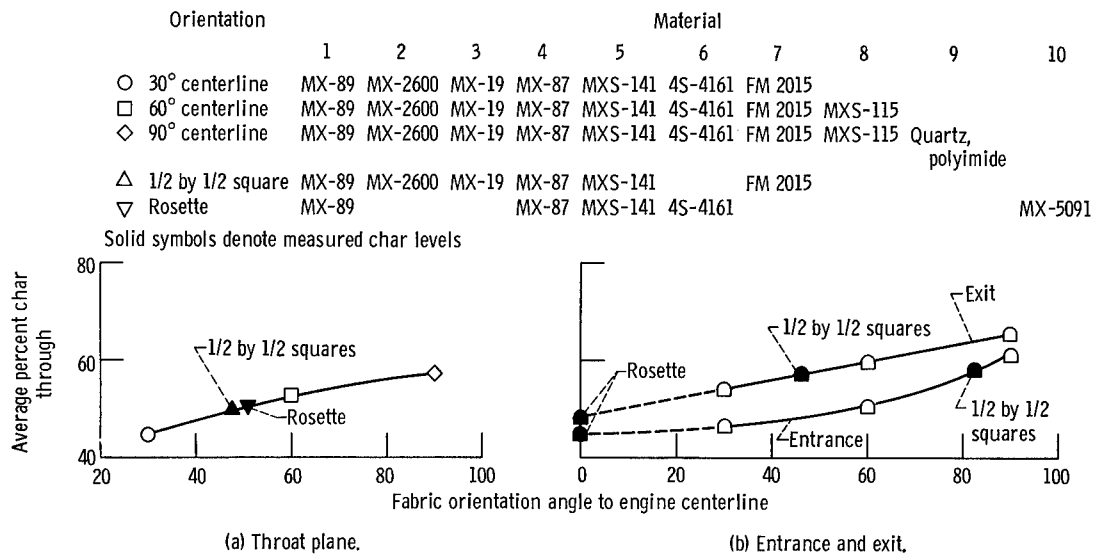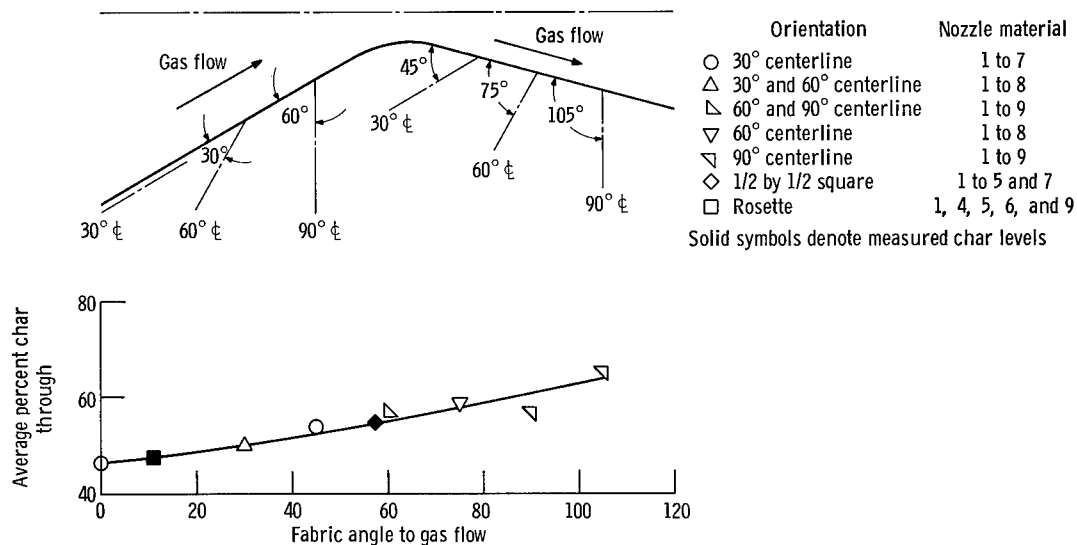
Figure 11. - Ablative char against fabric angle.

Figure 12. - Ablative char against fabric angle to gas flow.